

CMB foreground measurements through broad-band radio spectro-polarimetry: prospects of the SKA-MPG telescope

Aritra Basu,^{1,2*} Dominik J. Schwarz,¹ Hans-Rainer Klöckner,² Sebastian von Hausegger,³ Michael Kramer,² Gundolf Wieching² and Blakesley Burkhart^{4,5}

¹*Fakultät für Physik, Universität Bielefeld, Postfach 100131, D-33501 Bielefeld, Germany*

²*Max-Planck-Institut für Radioastronomie, Auf dem Hügel 69, D-53121 Bonn, Germany*

³*Niels Bohr Institute & Discovery Center, University of Copenhagen, Blegdamsvej 17, DK-2100 Copenhagen, Denmark*

⁴*Center for Computational Astrophysics, Flatiron Institute, 162 Fifth Avenue, New York, NY 10010, USA*

⁵*Department of Physics and Astronomy, Rutgers, The State University of New Jersey, 136 Frelinghuysen Rd, Piscataway, NJ 08854, USA*

Accepted to be published in the MNRAS on 2019 June 11

ABSTRACT

Precise measurement of the foreground synchrotron emission, which contaminates the faint polarized cosmic microwave background radiation (CMB), is a major challenge for the next-generation of CMB experiments. To address this, dedicated foreground measurement experiments are being undertaken at radio frequencies between 2 and 40 GHz. Foreground polarized synchrotron emission measurements are particularly challenging, primarily due to the complicated frequency dependence in the presence of Faraday rotation, and are best recovered through broad fractional-bandwidth polarization measurements at frequencies $\lesssim 5$ GHz. A unique opportunity for measuring the foreground polarized synchrotron emission will be provided by the 15-m SKA-MPG telescope operating in the frequency range 1.7 to 3.5 GHz (S-Band). Here, we present the scope of a Southern sky survey in S-Band at 1 degree angular resolution and explore its added advantage for application of powerful techniques, such as, Stokes Q , U fitting and RM-synthesis. A full Southern-sky polarization survey with this telescope, when combined with other on-going efforts at slightly higher frequencies, will provide an excellent frequency coverage for modeling and extrapolating the foreground polarized synchrotron emission to CMB frequencies ($\gtrsim 80$ GHz) with rms brightness temperature better than 10 nK per 1 degree². We find that this survey will be crucial for understanding the effects of Faraday depolarization, especially in low Galactic latitude regions. This will allow better foreground cleaning and thus will contribute significantly in further improving component separation analyses and increase usable sky area for cosmological analysis of the *Planck* data, and the *LiteBIRD* mission in the future.

Key words: cosmic microwave background – polarization – methods : data analysis – radio continuum : galaxies, ISM

1 INTRODUCTION

The cosmic microwave background (CMB) radiation is the first light observable after the Big Bang and is richly encoded with information on fundamental physics. Sensitive measurements of the CMB and its spatial anisotropies have been the most successful probe in our understanding of the Universe (Penzias & Wilson 1965; Smoot et al. 1992; Hinshaw et al. 2013; Planck Collaboration I et al. 2018). On

angular scales $> 1^\circ$, the next frontier in CMB experiments lies in the precise measurement of anisotropies in its polarization states, namely, the gradient-type E -mode and the curl-type B -mode, for the detection of primordial gravitational waves and imprints of reionization history of the Universe. A measurement of the B -mode signal from gravitational waves in the angular power spectrum of the polarized CMB on angular scales $\gtrsim 10^\circ$ (Polnarev 1985) could pin down the energy scale of cosmological inflation (Liddle 1994; Lyth 1997; Guo et al. 2011; Planck Collaboration X et al. 2018). Detection of *reionization bumps* on angular scales \gtrsim

* E-mail: aritra@physik.uni-bielefeld.de.

40°, in both the *E*- and *B*-modes, would give us information on the astrophysics and dark matter physics of the epoch of reionization (Zaldarriaga & Seljak 1997; Kogut et al. 2003).

Anisotropy studies of the CMB, both in intensity and polarization, from current space- and ground-based observations have revealed that the lack of proper foreground Galactic emission models is a bottle-neck in inferring orders of magnitude fainter cosmological signals. In total intensity, the foreground Galactic continuum emission consists of: synchrotron emission from relativistic electrons gyrating in ambient magnetic fields, bremsstrahlung (also referred to as the free-free emission) from thermal electrons scattering off ions, anomalous microwave emission (AME) and emission from thermal dust grains. In polarization, synchrotron and thermal dust emissions are the major contributors. Because each of these foreground components dominate in different frequency regimes, dedicated sky surveys are necessary to constrain them at their respective frequencies. Once constrained, they are then extrapolated to 60–250 GHz frequency range, where the relative contribution from the CMB is significant, and are subtracted. Hence, in order to measure CMB anisotropies with high precision, accurate understanding of the spectrum of each of the foreground emission components is imperative for subsequent extrapolation and subtraction at CMB frequencies.

The synchrotron and the free-free emissions dominate over the other foreground components at low radio frequencies and are therefore best constrained below 10 GHz. For a physical description of total and polarized synchrotron emission from the Milky Way, broad-bandwidth observations with multi-frequency coverage are necessary. Due to the lack of suitable large sky-area surveys below 10 GHz, current analyses typically rely on a mix of fits using power-laws, template maps and simulated spectra. Modelling of the total and polarized synchrotron spectrum is limited to minimal, empirical parametrization using the Haslam et al. (1982) all-sky survey at 408 MHz as a template, while the free-free emission is constrained by using ancillary Galactic $H\alpha$ maps (Dickinson et al. 2003; Planck Collaboration XXV et al. 2016; Planck Collaboration IV et al. 2018). To better constrain the polarized and total synchrotron emission, current efforts are targeting frequencies below 10 GHz, for example, the recent S-Band Polarization All Sky Survey (S-PASS) at 2.3 GHz (Krachmalnicoff et al. 2018; Carretti et al. 2019) and the on-going C-Band All Sky Survey (C-BASS) at 5 GHz (Jones et al. 2018).

Extrapolating the polarized synchrotron foreground to CMB frequencies from measurements at low radio frequencies ($\lesssim 10$ GHz) is especially challenging in the presence of Faraday rotation. This is because, depending on the properties of a magneto-ionic medium and how the synchrotron emitting and Faraday rotating plasmas are mixed, the polarized synchrotron emission varies in a complicated way, both with frequency and spatially. Imprints of complicated Galactic Faraday rotating medium on the polarized synchrotron emission spectrum is robustly captured through broad-bandwidth spectro-polarimetric observations, especially in the frequency range 2 to 10 GHz, and can be modelled with analytical descriptions of turbulent magneto-ionic media.

The upcoming SKA-MPG telescope, equipped with a sensitive receiver operating between 1.7 and 3.5 GHz (S-

Band) provides a unique opportunity to perform a broad-bandwidth, spectro-polarimetric survey of the entire Southern sky at 1° angular resolution. Although, the SKA-MPG telescope was not originally designed for CMB foreground studies, in this paper we explore the prospects of removal of foreground synchrotron and free-free emissions for a spectro-polarimetric survey performed at S-Band with it. The 1.75 GHz wide, continuous frequency coverage will offer a deeper understanding of the Milky Way’s radio continuum spectrum and the opportunity to constrain the Galactic total and polarized synchrotron emissions, along with the free-free emission from radio continuum data alone on a pixel-by-pixel basis.

This work is organized as follows. We briefly summarize the current scientific interest regarding CMB measurements in Section 2. In Section 3 we briefly discuss the present understanding regarding Galactic synchrotron emission from previous surveys. We present a physical approach to describe the total radio continuum foreground spectrum and discuss about effects of Faraday depolarization on polarized spectrum in Section 4. In Section 5 we present the specifications of the SKA-MPG telescope. In Section 6 we discuss the advantages of adding S-Band data in estimation of foreground contributions at CMB frequencies. In Section 7 we point out the possibility of a Southern-sky survey with the SKA-MPG telescope in the 12 to 18 GHz frequency range and discuss our findings in Section 8.

2 CMB FRONTIERS

Several decades of observational and theoretical efforts have established the CMB to be the most precise and advanced probe of cosmology. The Planck 2018 results give an excellent summary of the state of the art (Planck Collaboration I et al. 2018). The Universe can be described by the inflationary Λ cold dark matter (CDM) model, in which five cosmological parameters are measured at a level of accuracy better than one per cent. In this minimal model, only the reionization optical depth τ is constrained with a more modest accuracy of 10 per cent. Beyond the minimal model, upper limits on hypothetical new effects have been established, perhaps most impressive are tight upper limits on the curvature of the Universe and on the sum of the three neutrino masses.

A number of fundamental physics questions remain open and can be tackled by future CMB experiments. Those questions include — (1) is the cosmic structure seeded by quantum fluctuations during an epoch of cosmological inflation, or is there another mechanism at work?, (2) are there deviations from Einstein’s general relativity?, (3) what is the nature of dark matter and is the dark energy a cosmological constant?, (4) what is the origin of the matter-anti-matter asymmetry?, and (5) what are the neutrino masses? CMB also holds clues on important astrophysical questions, such as, (6) what reionized the Universe and how?, and (7) when did the first supermassive black holes form and how is their formation related to galaxy formation?

Here we focus on the aspects that can be addressed on the largest angular scales, as low-frequency foreground studies with single dish observations are limited in angular resolution by dish size. Answers and/or contributions to

questions (1), (2), (3), and (6) definitely require or will benefit from additional and improved information on large angular scales. The quest for the physics of inflation will profit tremendously from a possible detection of (or improved upper limits on) B -mode polarization caused by primordial gravitational waves. The history of reionization can be better constrained by a precise measurement of the so-called reionization bumps in the E - and B -mode angular power spectra. Deviations from general relativity can be constrained by probing primordial non-Gaussianity in the density fields on all angular scales. However, a detection of non-Gaussianity on larger angular scales would make it simpler to discriminate potential astrophysical effects that induce secondary non-Gaussian features on smaller angular scales. Hence, deviations from general relativity can be constrained via cross-correlations of the CMB temperature fluctuations with the large scale structure via the integrated Sachs-Wolfe effect on large angular scales.

Another motivation to aim at a better understanding of all CMB foregrounds is to disentangle several anomalies that have been observed in the CMB temperature anisotropies on large angular scales as compared to that predicted by the Λ -CDM model. These anomalies have been observed both with the *WMAP* and the *Planck* satellites (see [Bennett et al. 2011](#); [Planck Collaboration XVI et al. 2016](#); [Schwarz et al. 2016](#)), and therefore instrumental or analysis pipeline effects are less likely. Statistical significance of these anomalies is still inconclusive, i.e., they are seen at most around 3σ significance when investigated one by one, but the puzzling aspect is that there are several, seemingly unrelated and independent anomalous aspects. Among these are a lack of variance and angular correlation on the largest angular scales, alignment of phases of the lowest multipole moments with the Solar dipole and among each other (quadrupole-octopole alignment), hemispherical power asymmetry and power modulation and parity asymmetry. At least some of those anomalies could be due to yet unidentified features in the various CMB foregrounds. They will be further tested by CMB polarization experiments and might point towards unexpected new physics, unless foregrounds could eventually explain them.

To tackle these and other cosmological questions on large angular scales, the next generation of space missions is currently in preparation. Most advanced in the time line and funding effort is the Japan Aerospace Exploration Agency-led *LiteBIRD* mission ([Suzuki et al. 2018](#)) and plans exist in Europe and the US for a future large-scale CMB mission. Future ground-based CMB experiments will target smaller angular scales and will put their focus on dedicated fields in the sky. Many of them are on the Southern hemisphere, either at the South Pole or in the Atacama desert at high altitude. Currently the most ambitious project is CMB-S4 ([Abazajian et al. 2016](#)). The success of these missions and experiments will also depend on how well we understand CMB foregrounds, both in intensity and in polarization.

3 EXISTING OBSERVATIONS OF GALACTIC SYNCHROTRON POLARIZATION

To study the total Galactic synchrotron emission, several large sky-area surveys have been undertaken in the past at

frequencies below 5 GHz using narrow frequency bandwidths (e.g., [Berkhuijsen 1972](#); [Haslam et al. 1982](#); [Reich & Reich 1986](#); [Uyaniker et al. 1998](#); [Jonas et al. 1998](#), to mention a few). In polarization, most of the large sky-area surveys have been performed around 1.4 GHz (e.g., [Wolleben et al. 2006](#); [Testori et al. 2008](#)), and only a few surveys have gone up to 5 GHz ([Sun et al. 2007](#)).¹ Majority of these polarization surveys were not designed to constrain CMB foregrounds and were performed using narrow bandwidths at frequencies below 2 GHz. A combination of inadequate sensitivity and sky-coverage makes them unsuitable to glean complete information on the properties of the Galactic magneto-ionic medium and thereby for CMB foreground studies.

However, previous polarization surveys near 1.4 GHz have revealed that in the region along the Galactic plane, roughly within Galactic latitude (b) $|b| \lesssim 30^\circ$, the polarized emission is significantly depolarized ([Wolleben et al. 2006](#)). Depolarization could originate due to a combination of — frequency independent beam depolarization arising from turbulent magnetic fields on scales smaller than the telescope beam, and frequency-dependent Faraday depolarization due to the nature of the Galactic magneto-ionic medium. The latter can also give rise to strong spatial variations of the polarized synchrotron emission making it difficult to constrain its contribution at CMB frequencies. As a result, typically, the region $|b| \lesssim 20^\circ$ (roughly 30–40% of the total sky-area) is masked from CMB analyses. Among other things, this results in increased cosmic variance in the measurement of CMB angular power spectra on large angular scales which is of interest for next-generation CMB space missions.

The only all-sky Galactic Faraday depth (FD) distribution is available via interpolation of spatially discrete FDs measured towards extragalactic sources using Bayesian analysis ([Oppermann et al. 2012](#)). The Galactic FD varies widely from -500 to $+500 \text{ rad m}^{-2}$ in the region $|b| \lesssim 30^\circ$. In regions of such high FD, frequency-dependent Faraday depolarization increases towards lower frequencies and therefore the polarized Galactic emission in previous polarization surveys near 1.4 GHz were found to be depolarized. To mitigate the effects of Faraday depolarization and to accurately constrain the Galactic linearly polarized synchrotron emission at CMB frequencies, only recently efforts have turned towards the frequency range 2 to 10 GHz and to using wider frequency coverages. The frequency range 2.176 to 2.4 GHz is covered by the S-PASS and the 4.5 to 5.5 GHz is covered by the C-BASS. The advantage of performing polarization surveys at frequencies higher than 2 GHz to reduce the effects of Faraday depolarization has been demonstrated by the S-PASS data ([Carretti et al. 2013](#); [Krachmalnicoff et al. 2018](#)).

However, for $|b| \lesssim 30^\circ$, strong Faraday depolarization means that the polarized structures observed using the relatively narrow band of S-PASS are also expected to show strong spectral variations. A large frequency gap between S-PASS and C-BASS would make combining the S-PASS and C-BASS data a challenging proposition. In order to ro-

¹ For brief summary on previous large sky-area surveys using narrow frequency bands, we refer the interested reader to [Jones et al. \(2018\)](#) and <https://lambda.gsfc.nasa.gov/product/>.

bustly recover the polarized emission at low Galactic latitudes, wide bandwidth polarization survey using the SKA-MPG telescope, covering the 1.7 to 3.5 GHz range, will be crucial. In fact, the wide frequency coverage also allows us to constrain the Galactic total synchrotron emission spectrum using physically motivated models all over the Southern sky.

4 SYNCHROTRON AND FREE-FREE FOREGROUNDS

Each of the foreground emission components have distinct spectrum and dominates at different frequency regimes. Synchrotron emission typically has a steep power-law spectrum and dominates at frequencies $\lesssim 10$ GHz, while the thermal free-free emission has a flatter power-law spectrum which becomes significant above ~ 5 GHz. The AME spectrum has varying peaks in the frequency range 10–50 GHz. Thermal dust emission follows a modified Planck spectrum which starts to dominate above ~ 100 GHz. We refer interested readers to [Thorne et al. \(2017\)](#) and [Jones et al. \(2018\)](#) for details on foreground emission components. At frequencies above 10 GHz, where a wealth of foreground components become important, their modeling increasingly suffers from degeneracies giving rise to large uncertainties ([Planck Collaboration X et al. 2016](#)). Thus, to independently constrain the synchrotron and free-free emission components, observations below ~ 10 GHz are necessary, while AME and thermal dust emission are better constrained at frequencies above 10 and 100 GHz, respectively.

In order to constrain various low-frequency foreground components, dedicated surveys to map both total and polarized emissions are being performed, e.g., the C-BASS and the S-PASS at frequencies below 10 GHz, and the Q-U-I JOint TENERife (QUIJOTE; [Génova-Santos et al. 2015a,b](#)) and GreenPol² experiments in the 10 to 40 GHz frequency range. Short descriptions of these recent efforts are presented in Appendix A. In this paper, we will focus on constraining the total radio continuum emission below $\lesssim 10$ GHz and the polarized synchrotron emission from our Galaxy where observations in the S-Band with the SKA-MPG telescope will play an important role.

4.1 Total intensity spectrum

In the interstellar medium (ISM), the synchrotron-emitting relativistic electrons, also referred to as cosmic ray electrons (CREs), are believed to be accelerated in the shock fronts of supernova explosions via diffusive shock acceleration and are injected into the ISM with a power-law energy spectrum ([Bell 2004](#); [Jones 2011](#); [Edmon et al. 2011](#); [Kang et al. 2012](#)). As a consequence, the synchrotron emission arising from freshly injected CREs has a power-law frequency spectrum with slope β_{nt} .³ The value of β_{nt} depends on the Mach number (M) of the shock as, $\beta_{\text{nt}} = -(5M^2 - 1)/(2M^2 - 2)$ ([Blandford & Eichler 1987](#)). For strong shocks, i.e., $M \gg 1$,

$\beta_{\text{nt}} \approx -2.5$. However, since the Mach number depends on the sound speed and thereby the gas density of the medium where CREs are injected, β_{nt} could lie in the range -2.5 to -3 (see, e.g., [Caprioli & Spitkovsky 2014](#); [Park et al. 2015](#)).

Since injection, the CREs are subjected to energy dependent losses via various mechanisms, such as, ionization, relativistic bremsstrahlung, synchrotron and inverse-Compton (see e.g., [Longair 2011](#)). These losses affect different parts of the frequency spectrum and lead to the injected power-law synchrotron spectrum to be modified smoothly over a frequency range. Synchrotron and inverse-Compton losses typically dominate at frequencies $\gtrsim 2$ GHz which steepens the spectrum, and the nature of steepening depends on the process of particle injection. For example, beyond a break frequency ν_{br} the spectrum steepens from β_{nt} to $\beta_{\text{nt}} - 0.5$ in the case of continuous injection of CREs in an synchrotron emitting volume ([Pacholczyk 1970](#)). In the scenario when CREs in a volume are injected at a single epoch, the synchrotron spectrum either falls off as a power-law with index $(4\beta_{\text{nt}} - 1)/3$ for $\nu > \nu_{\text{br}}$ (KP model; [Kardashev 1962](#); [Pacholczyk 1970](#)) or develops an exponential cut-off at a cut-off frequency ν_{c} (JP model; [Jaffe & Perola 1973](#)).

Thus, to describe physical models of CRE energy losses, the synchrotron brightness temperature ($T_{\text{B,syn}}$) spectrum can be represented as,

$$T_{\text{B,syn}}(\nu) = T_{\text{syn},0} \frac{(\nu/\nu_0)^{\beta_{\text{nt}}}}{[1 + (\nu/\nu_{\text{br}})^{\gamma}]} e^{-(\nu/\nu_{\text{c}})}. \quad (1)$$

Here, $T_{\text{syn},0}$ is the brightness temperature normalization of the synchrotron emission at a pivot frequency ν_0 chosen such that $\nu_0 < \nu_{\text{br}}$ and $\nu_0 < \nu_{\text{c}}$, and γ is the spectral curvature parameter. Note that, in the case when $\nu_{\text{c}} \rightarrow \infty$, $\gamma = 0.5$ represents the scenario of continuous injection of CREs and $\gamma = (-\beta_{\text{nt}} + 1)/3$ represents the KP model. The JP model of CRE injections is given by a finite value of $\nu_{\text{c}} \lesssim \nu_{\text{br}}$.

The break- and cutoff-frequencies originating due to synchrotron and/or inverse-Compton cooling depends on the total magnetic field strength, the interstellar radiation field and age of the CREs in a way that, the older the CREs, the lower are ν_{br} and ν_{c} . The bulk of the CREs in galaxies is produced in galactic discs, roughly in a ± 500 pc region around galactic mid-plane. The CREs then propagate away from the galactic disc into the galactic halo via various transport mechanisms, such as, diffusion, streaming at Alfvén speed, galactic winds and/or advection (see e.g., [Heesen et al. 2016, 2018](#)). Depending on the dominant transport and diffusion mechanisms, CREs can take $\sim 10^6$ – 10^8 years to reach up to ~ 2 kpc or more above the mid-plane ([Krause et al. 2018](#)). Such transport time-scale of CREs in Galactic magnetic field strengths of 5–15 μG would result in ν_{br} and ν_{c} to typically lie in the range 2–10 GHz at high Galactic latitudes, $|b| \gtrsim 30^\circ$. At lower $|b|$, the CREs are expected to be young, and therefore ν_{br} and ν_{c} can lie at frequencies above 10 GHz. At an average, we expect break frequencies to decrease with increasing Galactic latitude $|b|$.

Spatially varying ISM conditions and magnetic field strengths give rise to locally varying breaks in the synchrotron spectrum which when averaged over large volume by a telescope beam could smooth-out the synchrotron spectrum ([Basu et al. 2015](#)). Also, mixing of different CRE populations via propagation and steady injection in the ISM would further smooth out any sharp spectral fall-off of the

² <https://www.deepspace.ucsb.edu/projects/greenpol>

³ In this paper, we will represent the frequency spectrum-slope (β) in terms of the brightness temperature (T_{B}), i.e., $T_{\text{B}}(\nu) \propto \nu^{\beta}$. The corresponding flux density spectrum $S(\nu)$ is given by, $S(\nu) \propto \nu^{\alpha}$ and α is related to β as $\alpha = \beta + 2$.

synchrotron emission as predicted by the KP and the JP models. Hence, in the Galactic ISM, we expect γ to lie in the practical range 0 and +2. Because of increasing CRE age and decreasing CRE injection rates with increasing $|b|$, steeper break in the synchrotron emission spectrum at high Galactic latitudes is expected. That means, in our parametrization for the synchrotron emission, γ is expected to increase with Galactic latitude $|b|$.

The Galactic free-free emission at frequencies above ~ 1 GHz is expected to be optically thin and follows a power-law spectrum with a spatially constant free-free spectral index $\beta_{\text{ff}} \approx -2.1$. Strictly speaking, β_{ff} is expected to decrease slightly with frequency due to frequency and electron temperature (T_e) dependent Gaunt factor (Bennett et al. 1992; Dickinson et al. 2003). At the frequencies of our interest, and for the typical range of T_e between 4000 and 10000 K in the Galactic ISM, the widely used approximate value of $\beta_{\text{ff}} = -2.1$ leads to systematic underestimation of the free-free emission by $\lesssim 2\%$ (Dickinson et al. 2003). Therefore, below 10 GHz, the total Galactic radio continuum emission $T_B(\nu)$ can be well described by,

$$\begin{aligned} T_B(\nu) &= T_{\text{B,syn}}(\nu) + T_{\text{B,ff}}(\nu) \\ &= T_{\text{syn},0} \frac{(\nu/\nu_0)^{\beta_{\text{nt}}}}{[1 + (\nu/\nu_{\text{br}})^{\gamma}]} e^{-(\nu/\nu_c)} + T_{\text{ff},0} (\nu/\nu_0)^{-2.1}, \end{aligned} \quad (2)$$

with six free parameters $T_{\text{syn},0}$, $T_{\text{ff},0}$ (normalization of the free-free emission at ν_0), β_{nt} , γ , ν_{br} and ν_c . $T_{\text{B,ff}}$ is the brightness temperature of the free-free emission. Large frequency coverage thereby provides the opportunity of constraining the Galactic synchrotron and free-free emission components directly from the total intensity radio continuum spectrum.

4.2 Complexities in the synchrotron polarization spectrum

Since the total intensity spectra of the different foreground components are smooth, once they are constrained at lower radio frequencies, e.g., between 5 and 40 GHz, it is simple to extrapolate them to higher frequencies around the dominant CMB emission, i.e., near 100 GHz. Extrapolation of the polarized emission, especially the polarized synchrotron emission measured at frequencies below 10 GHz is non-trivial due to the effects Faraday rotation and Faraday depolarization have on the polarized emission spectrum.

Faraday rotation describes the effect wherein the plane of polarization of a linearly polarized signal is rotated by an angle $\Delta\theta$ while traversing in a magneto-ionic medium and the observed angle of polarization (θ) at a wavelength λ is given by,

$$\theta(\lambda) = \theta_0 + \Delta\theta = \theta_0 + \text{FD} \lambda^2. \quad (3)$$

Here, FD is the Faraday depth and θ_0 is the intrinsic polarization angle of the linearly polarized signal, typically originating from synchrotron emission. In a purely Faraday rotating medium, the observed polarization angle varies linearly with λ^2 , and FD is given by its slope, which is also referred to as the Faraday rotation measure and is commonly denoted as RM. FD is the integral of the magnetic field component along the line of sight (B_{\parallel}) weighted by the thermal electron density (n_e), from the polarized source to an observer, and is

given by,

$$\text{FD} = 0.812 \int_{\text{source}}^{\text{observer}} \left(\frac{n_e(l)}{\text{cm}^{-3}} \right) \left(\frac{B_{\parallel}(l)}{\mu\text{G}} \right) \left(\frac{dl}{\text{pc}} \right) \text{ rad m}^{-2}. \quad (4)$$

In such a situation, the complex fractional polarization⁴ (p) varies with λ as,

$$p(\lambda) = p_0 e^{2i(\theta_0 + \text{FD}\lambda^2)}. \quad (5)$$

In typical astrophysical plasmas, e.g., those encountered in the Galactic ISM, Faraday rotating and synchrotron emitting plasmas are mixed, often leading to breakdown of the linear θ vs. λ^2 relation. In such scenarios, a part of the integral for FD in Eq. (4) is also contributed by a synchrotron emitting medium. The FD contributed by the part of a line of sight which is simultaneously Faraday rotating and synchrotron emitting will be denoted as FD_{em} . That is, the limits of the line integral in Eq. (4) spans from far to the near side of the synchrotron emitting volume only. In this paper, FD always represents the Faraday depth along the entire line of sight as given by Eq. (4), unless specified otherwise.

Further, depending on how the magnetic fields and free electrons are distributed in the plasma, p varies non-linearly with λ^2 and its analytical solutions under certain approximations are derived in detail by Sokoloff et al. (1998). The variation of p as a function of λ in a volume where synchrotron emission and Faraday rotation originate in uniform magnetic fields, known as the ‘Burn slab’ model (Burn 1966; Sokoloff et al. 1998), is given by,

$$p(\lambda) = p_0 \frac{\sin \text{FD}_{\text{em}} \lambda^2}{\text{FD}_{\text{em}} \lambda^2} e^{2i(\theta_0 + \frac{1}{2} \text{FD}_{\text{em}} \lambda^2)}. \quad (6)$$

If the volume is also clumpy and contains both turbulent and regular magnetic fields within which FD has a dispersion σ_{FD} , known as the internal Faraday dispersion model, the variation of p with λ is given by (Sokoloff et al. 1998),

$$p(\lambda) = p_0 e^{2i\theta_0} \left(\frac{1 - \exp[-(2\sigma_{\text{FD}}^2 \lambda^4 - 2i \text{FD}_{\text{em}} \lambda^2)]}{2\sigma_{\text{FD}}^2 \lambda^4 - 2i \text{FD}_{\text{em}} \lambda^2} \right). \quad (7)$$

Note that, it is possible that the magneto-ionic media described by equations (6) and (7) lies behind purely Faraday rotating media with Faraday depth FD_{fg} . Such cases be accounted for by multiplying these two equations by $\exp(2i \text{FD}_{\text{fg}} \lambda^2)$. FD defined in Eq. (4) is then $\text{FD} = \text{FD}_{\text{fg}} + \text{FD}_{\text{em}}$.

If a foreground Faraday rotating medium only contains turbulent magnetic fields, known as the external Faraday dispersion model, p varies with λ as (Sokoloff et al. 1998),

$$p(\lambda) = p_0 e^{-2\sigma_{\text{FD}}^2 \lambda^4} e^{2i(\theta_0 + \text{FD} \lambda^2)}. \quad (8)$$

The dispersion of FD, σ_{FD} , within the 3-dimensional volume probed by a telescope beam is related to the turbulent magnetic field along the line of sight, where B_{\parallel} has root-mean square (rms) b_{\parallel} , and properties of the magneto-ionic medium as,

$$\sigma_{\text{FD}} = 0.812 \left(\frac{\langle n_e \rangle}{\text{cm}^{-3}} \right) \left(\frac{b_{\parallel}}{\mu\text{G}} \right) \left(\frac{f_{\text{V}}^{-1} L l_c}{\text{pc}^2} \right)^{1/2} \text{ rad m}^{-2}. \quad (9)$$

⁴ Fractional polarization is defined as $p = PI/I_{\text{syn}}$, where PI and I_{syn} are the observed linearly polarized and total synchrotron intensities, respectively.

Here, $\langle n_e \rangle$ is the average density of thermal electrons with a volume filling factor of f_V . L is the path length through the ionized medium and l_c is the correlation length of the product $n_e b_{\parallel}$, referred to as the turbulent cell size. Depending on how turbulent energy is injected into the ISM of galaxies, l_c can be a few pc when driven by protostellar outflows, 50–100 pc when driven by supernovae, or a few kpc when driven by Galactic rotation, superbubble and/or Parker instability (see, e.g., [Armstrong et al. 1995](#); [Elmegreen & Scalo 2004](#); [Haverkorn et al. 2008](#); [Krumholz et al. 2018](#)). Therefore, for typical $b_{\parallel} \approx 10 \mu\text{G}$ and $L \approx 5 \text{ kpc}$, and depending on the location within the Galaxy, σ_{FD} can range from up to $\sim 10 \text{ rad m}^{-2}$ at high Galactic latitudes to 50–200 rad m^{-2} at low Galactic latitudes.

[O’Sullivan et al. \(2017\)](#) suggests a general description of all the above depolarizations in the presence of both regular and turbulent magnetic fields as,

$$p(\lambda) = p_0 \frac{\sin \Delta\text{FD} \lambda^2}{\Delta\text{FD} \lambda^2} e^{-2\sigma_{\text{FD}}^2 \lambda^4} e^{2i(\theta_0 + \text{FD} \lambda^2)}. \quad (10)$$

Here, ΔFD is the gradient of Faraday depth caused by variation of regular magnetic fields within the telescope beam.

In the case when the telescope beam probes a large volume of an astrophysical system, a combination of the above mentioned plasma conditions are observed. Therefore, in order to model the observed variation of $p(\lambda)$, one linearly combines these models and direct fitting of the Stokes Q and U intensity spectra is performed known as the Stokes Q , U fitting. Of late, with the acquisition of broad band radio polarimetric data, the technique of Stokes Q , U fitting has been applied to infer properties of the magneto-ionic medium in different types of extragalactic objects, e.g., active galactic nuclei ([O’Sullivan et al. 2012](#); [O’Sullivan et al. 2017](#); [Pasetto et al. 2018](#)), external galaxies ([Shneider et al. 2014](#); [Mao et al. 2015](#)) and high redshift galaxies ([Kim et al. 2016](#); [Mao et al. 2017](#)).

The technique of Stokes Q , U fitting is a powerful tool for extrapolating polarized emission observed at low radio frequencies to arbitrarily high frequencies. However, for robust fits, large λ^2 -coverage through broad bandwidth polarization measurements is necessary, without which the fitted models and their parameters could be degenerate giving rise to large systematic uncertainties. Further, since Faraday depolarization depends strongly on λ , polarization measurements at small λ or high frequencies ($\gtrsim 5 \text{ GHz}$) often do not adequately capture the depolarization features in the polarized emission spectrum introduced by multiple components and are therefore insufficient. At low Galactic latitudes, $|b| \lesssim 30^\circ$, strong Faraday depolarization gives rise to strong spectral and spatial variations of the polarized synchrotron emission. Therefore, at longer λ , i.e., frequencies $\lesssim 1 \text{ GHz}$, Faraday depolarization is severe leading to either very little polarized signal or the observed polarized emission originating locally (e.g., [Jelić et al. 2015](#)). These issues necessitates broadband polarization survey in the frequency range 2 to 5 GHz.

5 THE SKA-MPG TELESCOPE

The SKA-MPG telescope, shown in Fig. 1, is a 15-m aperture offset-Gregorian telescope being constructed by the MT



Figure 1. A schematic view of the SKA-MPG telescope which is being constructed in the Karoo desert, South Africa.

Mechatronics GmbH in collaboration with the Max-Planck-Institut für Radioastronomie (MPIfR) of the Max Planck Society (MPG). This telescope is the first prototype dish of the South African Square Kilometre Array (SKA)-MID component that is being assembled in the Karoo desert, South Africa. The location of the telescope is offset with respect to the positions of the MeerKAT- and SKA-MID-configuration and is specially suited for a critical system design review and an independent scientific programme. The telescope will be equipped with S- and Ku-Band receiver systems, both developed by the MPIfR (for details see Table 1). The S-Band receiver covers 1.7 to 3.5 GHz and the Ku-Band receiver covers 12 to 18 GHz, and depending on the scientific merit additional frontends could be installed in the future.

In general, the benefits of an offset-Gregorian design are: an increased gain due to no aperture blockage, a reduction of standing waves in the aperture, and a reduction of stray radiation and possibly radio frequency interference (RFI). A disadvantage of this design is an asymmetric primary beam that may require a more complex calibration procedure. However in the telescope design phase special care has been taken to optimize the primary beam properties. Theoretical modelling indicates a well behaved primary beam having an ellipticity of 0.022, and the first and the second sidelobes are at -24 and -32.8 dB , respectively, at the centre frequency 2.6 GHz in S-Band. Until a full characterization of the system, only the theoretical limits are provided. The collecting area of the SKA-MPG telescope depends on the optical path between the primary and the secondary reflector system and its shaped optics is optimized to an effective area equivalent to a 15-m dish. This will provide us angular resolutions between 50 to 25 arcmin at the lowest and the highest frequency of the S-Band, respectively (see Table 1). Therefore, the lowest frequency limits the angular

Table 1. Expected specifications of the SKA-MPG telescope.

	S-Band	Ku-Band
Location	Karoo, South Africa	
Coordinates	30° 43′ 4.69″S, 21° 24′ 47.02″E	
Antenna	15-m offset-Gregorian	
Rx frequency	1.7–3.5 GHz	12–18 GHz
Digitizer bandwidth per Stokes	1.75 GHz (12-bit)	3 GHz (12-bit)
Frequency channels	1024 or 2048	2048
Polarizer	Linear	Circular
Stokes	(< -35 dB cross coupling before calibration) <i>I, Q, U, V</i>	
Beam FWHM [†]	$T_{\text{sys}} < 20$ K 50–25 arcmin	$T_{\text{rec}} < 18$ K 7–4.6 arcmin
Total intensity confusion [†]	300–50 mJy (16–2 mK)	1.7–0.6 mJy (80–28 μ K) ^a
Stokes <i>Q</i> & <i>U</i> confusion:		
Polarized sources ^{†,b}	1.7–0.23 mJy (90–9 μ K)	7.5–2.4 μ Jy (0.40–0.12 μ K)
Polarization leakage ^{†,c}	0.6–0.1 mJy (32–4 μ K)	3.4–1.2 μ Jy (0.16–0.06 μ K)
Typical integration required: [‡]		
Total intensity	30 second	≈ 10 minute
Stokes <i>Q</i> & <i>U</i>	2 hour	–
Faraday depth FWHM	≈ 140 rad m ⁻²	≈ 10 000 rad m ⁻²
Maximum Faraday depth	≈ ±4 × 10 ⁴ rad m ⁻²	≈ ±6.5 × 10 ⁵ rad m ⁻²
Faraday depth scale	≈ 450 rad m ⁻²	≈ 10 000 rad m ⁻²

[†] The range corresponds to values at the lowest and the highest frequency end of the receiver.

^a The confusion noise limit at Ku-Band was estimated by assuming the same source distribution as that at S-Band and a typical spectral index of -2.7 for extragalactic sources.

^b Confusion from polarized sources is calculated based on [Loi et al. \(2019\)](#).

^c Assuming a conservative on-axis instrumental leakage up to 0.2% on unpolarized regions.

[‡] For reaching confusion noise over 10 MHz channel-width per beam at S-Band and 1 GHz channel-width at Ku-Band.

resolution of sky survey using the SKA-MPG telescope to 1 degree.

Both S- and Ku-Band receiver systems follow the classical design of cryogenic cooled receivers, with a room-temperature linear feed for the S-Band and a cryogenic circular feed for the Ku-Band system. Both systems are equipped with a 12-bit, temperature stabilized, internal digitizer that operates on 2 Stokes × 1.75 GHz and 2 Stokes × 3 GHz bandwidth in S- and Ku-Band, respectively. Thus, the SKA-MPG telescope will provide an instantaneous bandwidth of 1.75 GHz in the S-Band and 3 GHz in the Ku-Band. After the digitizer, the data stream is structured by the packetizer, with an optional bandwidth reduction, before it is transported to the central processing building. In the final post processing step, the properties of the data products are freely choosable within computational limits and can be optimized for each individual observation. As an example, the variable configuration allows for a maximum of 2048 channels over the entire frequency bands. The anticipated system stability may reach a dynamic range of the order of 35 dB or better and a system temperature (T_{sys}) below 20 K in S-Band and receiver temperature (T_{rec}) below 18 K in Ku-Band. The expected setup of the data products are summarized in [Table 1](#).

5.1 Sensitivity

In [Fig. 2](#), we show the expected sensitivity of the SKA-MPG telescope over its S-Band frequency coverage for $T_{\text{sys}} = 20$ K. The different coloured bands are for different integration times per resolution element averaged over 1 MHz (top edge of each colour) to 10 MHz (bottom edge of each colour). Low-frequency single-dish surveys are limited by confusion noise in total intensity arising from unresolved sources and is expected to be in the range of 2 to 15 mK (the solid black line in [Fig. 2](#)) at the frequency and resolution of the SKA-MPG telescope. The confusion limit can be achieved in just 30 seconds for 10-MHz wide frequency channels over the entire S-Band. Assuming a close to uniform sky-coverage, a total-intensity-confusion limited survey of the Southern sky (an area of ≈ 21 000 deg²), can be performed in about 300 hours⁵ (including astronomical calibration overhead of 20%) making SKA-MPG telescope an excellent, fast, sky-survey instrument. In polarized intensity, however, due to the lack of bright polarized sources, the confusion noise is expected to be at < 0.1 mK level (following [Stil et al. 2014](#); [Loi et al.](#)

⁵ Here we have considered the possibility of a non-uniform sky coverage in terms of the integration time due to scanning overlaps. The estimated time also includes, in about 15% of the sky, at an average, the integration time is increased by a factor of five.

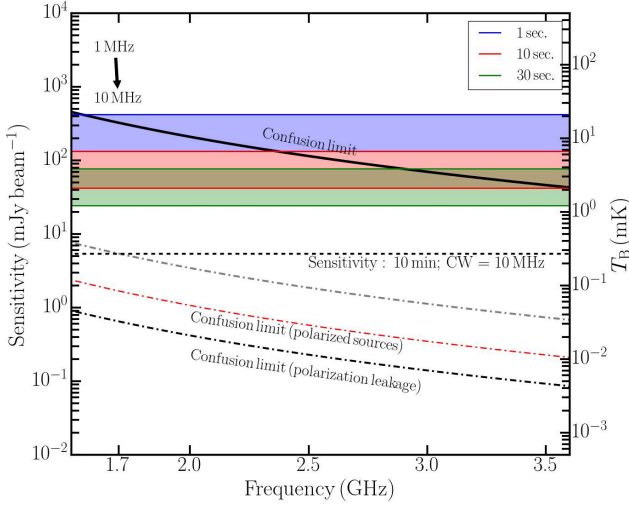


Figure 2. Expected sensitivity limits of SKA-MPG telescope. The solid black curve show the total intensity confusion limit and the black dash-dot curve is the confusion in Stokes Q and U assuming 0.2% instrumental polarization leakage. The red dash-dot curve shows the confusion arising from polarized sources. The grey dash-dot curve is for $3\times$ the total confusion noise in polarization. The various bands show the range of sensitivity expected for integration time of 1 second (blue), 10 seconds (red) and 30 seconds (green). The upper edge for each band is averaging over 1 MHz and the bottom is for averaging over 10 MHz. The black dashed line is the sensitivity for 10 MHz averaging and an integration time of 10 minutes (see Section 5.1).

2019) over the entire S-Band and hence deeper sensitivity to polarized emission can be achieved with longer integration.

In S-Band, a sensitivity of ~ 2 mK is sufficient for detecting diffuse polarized emission from the entire Southern-sky as suggested by the S-PASS at 2.3 GHz (see Krachmalnicoff et al. 2018; Carretti et al. 2019). However, to robustly apply the Stokes Q, U fitting technique, a signal-to-noise ratio (SNR) > 5 is required per frequency channel (Schnitzeler 2018). Hence, the target is to achieve sensitivity of 0.3 mK in Stokes Q and U , averaged over 10 MHz channel-width across the entire S-Band. We note that, due to frequency dependent variation of the polarized intensity at $|b| \lesssim 30^\circ$, SNR per 10-MHz channel could vary. At $|b| \gtrsim 30^\circ$, as Faraday depolarization is expected to be low, the polarized intensity is expected to follow a close to power-law spectrum. Therefore, the Galactic polarized emission in the higher frequency-end of S-Band could be weaker compared to the representative value of sensitivity at 2.3 GHz used by us. In those regions, to achieve higher SNR, we can afford to average to 40-MHz channel-widths or more without being significantly affected by channel-width depolarization.

Achieving a sensitivity of 0.3 mK in the polarized intensity, also necessary for better foreground removal for CMB related studies, will require about 10 minutes averaged over 10 MHz (see Fig. 2) per resolution element. A close-to 10 MHz channel-width will be achieved by averaging 10–12 channels, i.e., about 200 frequency channels spread over the S-Band coverage of the SKA-MPG telescope. To reach the requisite sensitivity, the Southern sky will be covered

20 times, each time performing a 300-hour total-intensity-confusion limited survey.

5.2 Observational challenges

Single dish telescopes are ideal for performing large sky-area surveys as they are sensitive to diffuse emission on all angular scales, unlike interferometers which suffer from missing emission structures on scales larger than the resolution of the shortest baseline. However, single dish observations face challenges from systematics arising because of the additive nature of recording signals. A full description of the survey strategy and characterization of the telescope properties are beyond the scope of this paper. They will be presented in detail in another paper after the construction of SKA-MPG telescope is completed and is ready for scientific commissioning. Here we discuss in brief about the features of the SKA-MPG telescope in coping with the observational challenges.

Scanning: In order to recover diffuse emissions and map them accurately, usual scanning artefacts are mitigated by performing cross-linked scans and applying the technique of basket-weaving. To optimize time efficiency and telescope slewing for large sky-area surveys, long scans along the telescope’s azimuthal direction at a fixed elevation is performed (see, e.g., Carretti et al. 2019; Jones et al. 2018). This type of long azimuthal scans typically results in non-uniform sky coverage in terms of integration time. One way to achieve close to uniform sky coverage is to perform azimuthal scans fixed at several elevation angles and driving the telescope at faster speeds in regions of multiple scan overlap. The SKA-MPG telescope offers a maximum slewing speed of 3° s^{-1} along the azimuthal axis and 1° s^{-1} along the elevation axis. The automatic control unit on the telescope allows position determination on a $50 \mu\text{s}$ time-scale, allowing us to achieve sky-scanning speed close to the maximum slewing speed. However, practical time-scales for telescope position determination depend on the dish tracking operations and the frequency of the status message update. These can be optimized based on the needs of the observing programme. We are currently exploring different scanning strategies to optimize the total survey time to cover the sky as uniformly as possible. Depending on the scanning strategy, it is possible that the time-scale of each total-intensity-confusion limited survey presented in Section 5.1 can go up by up to a factor of two.

Ground spillover: Single dish telescopes are prone to pick up stray emission from the ground, especially when observing at low telescope elevation. This is even more true for an offset-Gregorian feed as used for the SKA-MPG telescope. The ground spillover can be significantly reduced by extending the sub-reflector to the bottom. For the SKA-MPG telescope an extension of 40° has been selected (I. P. Theron, SKA-TEL-DSH-0000018, Rev 2, Dish Optics Selection Report) which will reflect any spillover towards the sky. We therefore believe that the pick up emission from the ground at low telescope elevations will be low for the survey.

Calibration: Novel designing of the S-Band receiver on the SKA-MPG telescope provides spectroscopic Allan time of $\gtrsim 1000$ seconds having wide band gain stability with rms better than 0.03%. This considerably reduces the frequency

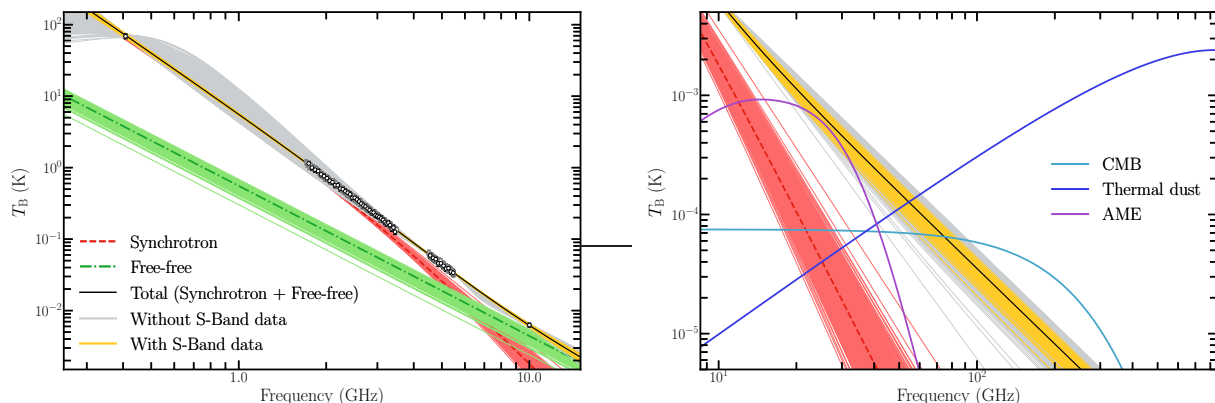


Figure 3. *Left:* An example total radio continuum frequency spectrum is shown as the solid black line. The red dashed line is the synchrotron emission spectrum with $\nu_{\text{br}} = 4$ GHz normalized to 5 K at 1 GHz, the green dot-dashed line is the free-free emission spectrum with a thermal fraction of 10% at 1 GHz. The data points are simulated measurements at 408 MHz, S-Band, C-Band, and 10 GHz with noise. The coloured lines show fits to 500 random realizations of simulated data using Eq. (2). The yellow and grey lines are for fits with and without the S-Band data, respectively. *Right:* Fits in the left panel extrapolated to higher frequencies. To highlight the recovered synchrotron + free-free emission, the extrapolated free-free component fits are not shown. For comparison, we show the spectrum of the CMB total intensity rms as the light-blue line. The foreground AME and thermal dust emission is shown as the magenta and dark blue lines, respectively. All the other lines have the same meaning as in the left panel.

of performing calibration on astronomical sources and system gains can be calibrated using the internal polarized noise generator on the S-Band receiver. Since the SKA-MPG telescope has linear polarizations, calibrating linearly polarized signal is expected to be challenging. However, the low on-axis cross-coupling of < -35 dB to circular polarization will reduce the challenge of calibrating linear polarizations. The exact performance of SKA-MPG telescope will be tested during its commissioning.

6 ADVANTAGES OF A NEW S-BAND SURVEY

In this section, we discuss the main advantages of having broad bandwidth spectro-polarimetric data in S-Band along with C-Band data from the C-BASS for constraining the polarized synchrotron emission. We use additional lower and higher frequency data, at 408 MHz and around 10 GHz, respectively, for constraining the total synchrotron and free-free emissions.

6.1 Recovering synchrotron and free-free emission foregrounds

Following the motivation discussed in Section 4.1, we adopt Eq. (2) to model the total intensity radio continuum emission below 10 GHz in our Galaxy, i.e., as a sum of synchrotron emission ($T_{\text{B,syn}}$) and an optically thin free-free emission ($T_{\text{B,ff}}$) — so far only used in the characterization of other galaxies’ radio spectra (see, e.g., Paladino et al. 2009; Tabatabaei et al. 2017; Klein et al. 2018). Since sharp spectral steepening is somewhat unlikely in galactic ISM, we assume a fixed $\nu_c \gg 10$ GHz, which leads to setting the exponential-term in Eq. (2) to unity. It is obvious that with either $\nu_{\text{br}} \rightarrow \infty$ or $\gamma = 0$ we arrive back at an addition of two simple power-law spectra.

To assess the importance of having new broad-bandwidth data in the S-Band, here we simulate a synthetic radio continuum spectrum and apply Eq. (2) to constrain the contribution of synchrotron and free-free emission components to the CMB. In the left-hand panel of Fig. 3, we generate a model of the total radio continuum emission (shown as the solid black line) in a 1×1 deg² pixel with a curved synchrotron emission component (shown as the red dashed line) and an optically thin free-free emission component (shown as the green dot-dashed line). The synchrotron emission has spectral index $\beta_{\text{nt}} = -2.8$ and a break at $\nu_{\text{br}} = 4$ GHz, similar to values found in Klein et al. (2018). The spectral curvature γ was fixed at $\gamma = 1.5$ — a somewhat strong break, yet illustrative for our purpose. The synchrotron brightness is normalized to 5 K at 1 GHz (a somewhat bright region in the sky) for a 1×1 deg² patch of sky, roughly corresponding to the angular resolution of the SKA-MPG telescope. The free-free emission component is normalized to 10% of the total emission at 1 GHz, a typical value observed in spatially resolved nearby galaxies (Basu et al. 2012). The fictive measurements are performed at C-Band (4.5 to 5.5 GHz) divided into 128 channels using the specifications of the Southern-sky survey of C-BASS listed in table 2 of Jones et al. (2018), and at S-Band (1.7 to 3.5 GHz), using the specifications of SKA-MPG telescope listed in Table 1 with 200 channels. In addition, we include a data point at Haslam’s 408 MHz with an uncertainty of 1 K and one from a QUIJOTE- or GreenPol-like experiment at 10 GHz with an uncertainty of 25 μ K, consistent with their specifications (see also Section 7).

We generated 500 data realizations with the input model, Eq. (2), wherein the data points in each case were randomly drawn from a Gaussian noise distribution. The noise for each data point includes: respective survey sensitivity, confusion noise and a calibration error of 2% was added to highlight the robustness of our results in light of real data. The yellow and grey lines in Fig. 3 (left panel)

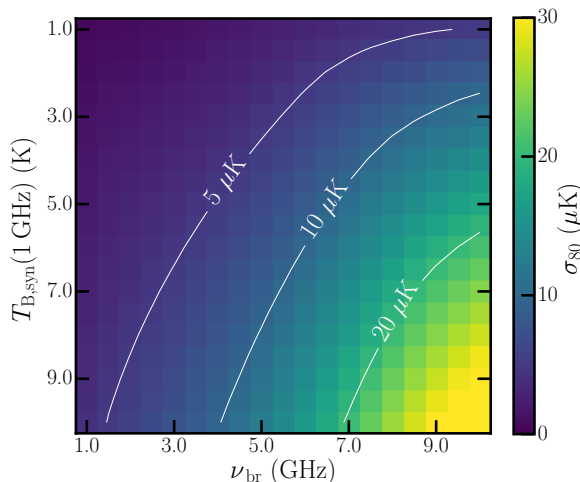


Figure 4. Dispersion σ_{80} of model fits using Eq. (2) around the expected synchrotron + free-free emission at 80 GHz for various choices of ν_{br} and synchrotron normalizations ($T_{\text{B,syn}}$) at 1 GHz for the case when S-Band data are included.

show the result of fitting *with* and *without* the S-Band data, respectively. The red and the green lines show the recovered synchrotron and free-free emissions, respectively, when S-Band data are included. This demonstrates the possibility of separating the synchrotron and free-free emission components using multi-frequency radio continuum data alone.

In the right-hand panel of Fig. 3 we show the extrapolations of the recovered spectra in the vicinity of 80 GHz, relevant for CMB experiments. For a comparison, the typical contribution of other foreground components, AME and thermal dust, and the expected rms brightness temperature fluctuations of the CMB are plotted as the different solid lines. The parameters describing the AME and the thermal dust emission are taken from table 5 of Jones et al. (2018) and are representative of a $1 \times 1 \text{ deg}^2$ patch of the sky where the foregrounds are significant, i.e., for $|b| \lesssim 20^\circ$. It should be noted that while the fits ‘with S-Band’ follow the true signal closely, those ‘without S-Band’ are distributed bi-modally around the true values with biases on both sides.⁶ Further note that, we have not fitted the other foreground components and they are shown only for reference. In this example, the dispersion of the brightness temperature (σ_{80}) of the recovered synchrotron + free-free emission around the expected value at 80 GHz decreases from $\sim 25 \mu\text{K}$ without the S-Band data to $< 10 \mu\text{K}$ by including the S-Band data.

In Fig. 4, we show σ_{80} as colour for various values of break frequencies ν_{br} and synchrotron normalizations at 1 GHz, $T_{\text{B,syn}}(1 \text{ GHz})$. For the typical range of values both these parameters can have, synchrotron + free-free emission can be recovered with rms better than $30 \mu\text{K}$ at 80 GHz. Low brightness temperature, $T_{\text{B,syn}}(1 \text{ GHz}) < 5 \text{ K}$, typically represent regions of high Galactic latitude for which we find the residuals to be $\lesssim 5 \mu\text{K}$. It is in these regions of the sky where ν_{br} and ν_{c} are expected to be between 2 and 10 GHz.

⁶ Given the steep spectrum of the synchrotron emission above $\sim 10 \text{ GHz}$, the total emission at 80 GHz is essentially only free-free. It is the bias in the free-free emission seen in the right-hand-side panel.

Therefore, new broadband measurements between 1.7 and 3.5 GHz with the SKA-MPG telescope will be important in constraining the synchrotron spectrum also at high Galactic latitudes.

In bright regions with ν_{br} lying above $\sim 7 \text{ GHz}$, i.e., the yellow region in the bottom right part of Fig. 4, the residuals increase to more than $20 \mu\text{K}$. The CREs in the bright regions of our Galaxy, i.e., close to the mid-plane region, are likely to be young and ν_{br} can lie above 10 GHz (see Section 4.1), even up to 100 GHz for CREs accelerated in supernovae remnants which exploded $< 10^5$ years ago. Thus, in order to pin down the synchrotron spectra in regions where ν_{br} lies above 10 GHz, additional data in the Ku-Band and higher frequencies, in the range 10 to 40 GHz, will be useful, provided the increased AME contribution at those frequencies is also modeled with sufficient accuracy. Therefore, with the parametrization of the radio continuum emission below 10 GHz by Eq. (2), we expect to recover the foreground synchrotron + free-free emission around 80 GHz with rms $\lesssim 10 \mu\text{K}$ per 1 deg^2 in most parts of the sky.

6.2 Recovering the polarized synchrotron foreground

Current, large sky-area surveys for measuring the polarized synchrotron foreground using broad bandwidths, are either performed at too low frequencies or at too high frequencies, severely limiting the scope of robustly determining the effects of Faraday depolarization and applying Stokes Q , U fitting (see Appendix A). A spectro-polarimetric survey in S-Band using the SKA-MPG telescope will provide the perfect opportunity to bridge the large frequency gap between the C-BASS and the existing S-PASS. This opens up the possibility to apply the technique of RM-synthesis (Brentjens & de Bruyn 2005) and directly produce a Galactic Faraday depth map without relying on Bayesian techniques applied to Faraday depths measured for discrete extragalactic sources (Oppermann et al. 2012; Oppermann et al. 2015).

The 1.7 to 3.5 GHz frequency coverage of SKA-MPG telescope will provide high Faraday depth resolution with rotation measure spread function (RMSF) FWHM of $\approx 140 \text{ rad m}^{-2}$ in contrast to $\approx 2400 \text{ rad m}^{-2}$ for C-BASS. The RMSFs for the two frequency coverages, and for comparison, a combination of the C-BASS and the S-PASS frequencies are shown in the left-hand panel of Fig. 5. In the right-hand panel of Fig. 5, the corresponding deconvolved (or cleaned) RMSFs are shown. Note that, for the combined S-PASS+C-BASS data, residual sidelobes at 15 per cent level are seen. The accuracy (δFD) to which FD can be estimated is related to the FWHM of the RMSF as, $\delta\text{FD} = \text{FWHM}/(2\text{SNR})$, where SNR is the signal-to-noise ratio of the linearly polarized intensity. This relation is applicable to the simple scenario when there is a single FD component within the RMSF peak, or for a synchrotron emitting and Faraday rotating medium which has $\text{FD} \ll \text{FWHM}$ and/or $\sigma_{\text{FD}} \ll \text{FWHM}$.

Since, the resolution of FD in C-Band is poor, C-BASS data alone would be inadequate to distinguish complicated and/or wide Faraday depth structures in the Faraday depth spectrum originating due to Faraday depolarization (see Section 4.2). Moreover, it also limits the accuracy to which the polarization angle measured using the C-BASS data can

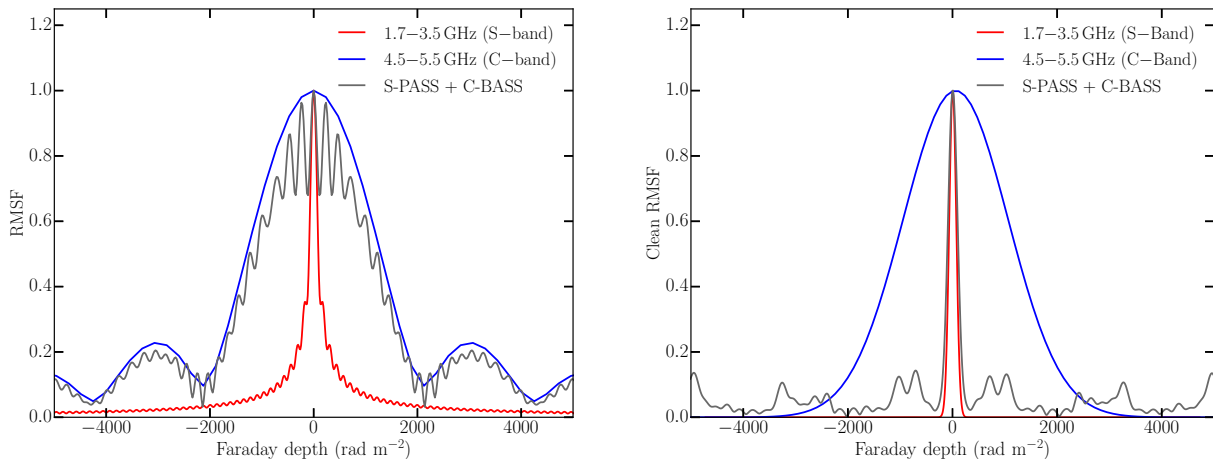


Figure 5. *Left:* Rotation measure spread function (RMSF) for the S-Band frequency coverage of SKA-MPG telescope is shown in red and has $\text{FWHM} \approx 140 \text{ rad m}^{-2}$. RMSF with $\text{FWHM} \approx 2400 \text{ rad m}^{-2}$ for C-Band frequency coverage of C-BASS is shown in blue. The grey RMSF is for a combination of S-PASS and C-BASS frequencies with the same frequency weighting. *Right:* Deconvolved (or cleaned) RMSFs for the corresponding frequency coverages shown in the left-hand panel.

be corrected for Faraday rotation. Combining C-BASS and S-PASS data would improve FD measurements for sources with simple Faraday depth spectra, e.g., at high Galactic latitudes ($|b| \gtrsim 30^\circ$). But, sources extended in Faraday depth would suffer from inaccurate flux recovery due to the 15 per cent sidelobes of the deconvolved RMSF (see Fig. 5). This will be severe at $|b| \lesssim 30^\circ$. With the availability of broadband data at S-Band using the SKA-MPG telescope, we will be able to measure Faraday depths at better than $\sim 15 \text{ rad m}^{-2}$ accuracy up to Faraday depths of $\pm 4 \times 10^4 \text{ rad m}^{-2}$ and be sensitive to extended Faraday depth structures up to $\sim 450 \text{ rad m}^{-2}$. This would allow us to measure complicated Faraday depth structures (Frick et al. 2011) from the turbulent interstellar medium at low Galactic latitudes and also produce a robust Southern-sky Faraday depth map.

6.2.1 Regions of high Faraday depolarization

Note that, RM-synthesis is an important tool to recover polarized signals that are otherwise too faint to be detected at the sensitivity level of individual narrow channels and/or could suffer from significant depolarization when averaged over large bandwidths. However, interpreting complicated Faraday depth spectra to recover the intrinsic polarization angle and fractional polarization is difficult (see e.g., Anderson et al. 2016). The technique of direct fitting of the observed Stokes Q and U spectra with analytic models of turbulent magneto-ionic medium offers a better solution to study a Faraday complex medium. To demonstrate the power of Stokes Q , U fitting, here we show an example using a synthetic polarization spectrum constructed from a magnetohydrodynamic (MHD) simulation of turbulent ISM.

Polarization observations of the Galactic plane have revealed the turbulence in the warm diffuse phase of interstellar gas to be low sonic Mach number through comparisons with MHD simulations of isothermal compressible turbulence (Burkhart et al. 2009; Gaensler et al. 2011; Burkhart et al. 2012; Herron et al. 2016). The sub-sonic nature of ISM turbulence in the warm/hot phases has also

been confirmed through Galactic HI 21-cm observations (Burkhart et al. 2010; Koley & Roy 2019). Here, we use the same MHD simulation of a $512 \times 512 \times 512 \text{ pc}^3$ volume having mesh resolution of $1 \times 1 \times 1 \text{ pc}^3$ from Burkhart et al. (2009, 2013).⁷ The simulation consists of a background magnetic field of strength $10 \mu\text{G}$ in the plane of the sky, and the ratio of ordered to turbulent magnetic field strengths is ~ 2 . The median electron density (n_e) in the simulation volume is 0.1 cm^{-3} and has a maximum value of $\sim 3.5 \text{ cm}^{-3}$. Faraday depth integrated along the line of sight varies between -350 and $+350 \text{ rad m}^{-2}$ per $1 \times 1 \text{ pc}^2$ pixel. Such values of n_e and FD are typically encountered in the thin disc of the Milky Way, roughly within $|b| < 20^\circ$ (see Cordes & Lazio 2003; Oppermann et al. 2012, respectively).

Synthetic broadband observations of the linearly polarized synchrotron emission including the effects of Faraday rotation were generated for the above mentioned simulation (A. Basu et al. in preparation). The Stokes Q and U parameters were calculated for a 512 pc long line of sight and averaged over $30 \times 30 \text{ pc}^2$. This set-up corresponds roughly to a $1 \times 1 \text{ deg}^2$ patch on the sky at a distance of 10 kpc , the typical distance in the Galaxy and roughly matched to the angular resolution of a survey with the SKA-MPG telescope.

We generated values for Stokes Q and U in the frequency ranges, 1.7 to 3.5 GHz (S-Band covered by SKA-MPG telescope) divided into 200 frequency channels, 4.5 to 5.5 GHz (C-Band covered by C-BASS in the South) divided into 128 frequency channels and some around 80 GHz, i.e., a representative high frequency near which the CMB polarized foreground is to be estimated. Stokes Q , U values near 80 GHz were computed to compare results of extrapolation and were not used for fitting. Sensitivity of the respective surveys, a calibration error of 2% and confusion noise from polarized sources were added as Gaussian noise to the Stokes Q and U data in the S- and C-Bands. The total synchrotron emission was normalized to 1 K at 1 GHz for the 1 deg^2 patch of

⁷ For details on the numerical setup, see Kowal et al. (2007), Burkhart et al. (2009) and Bialy et al. (2017).

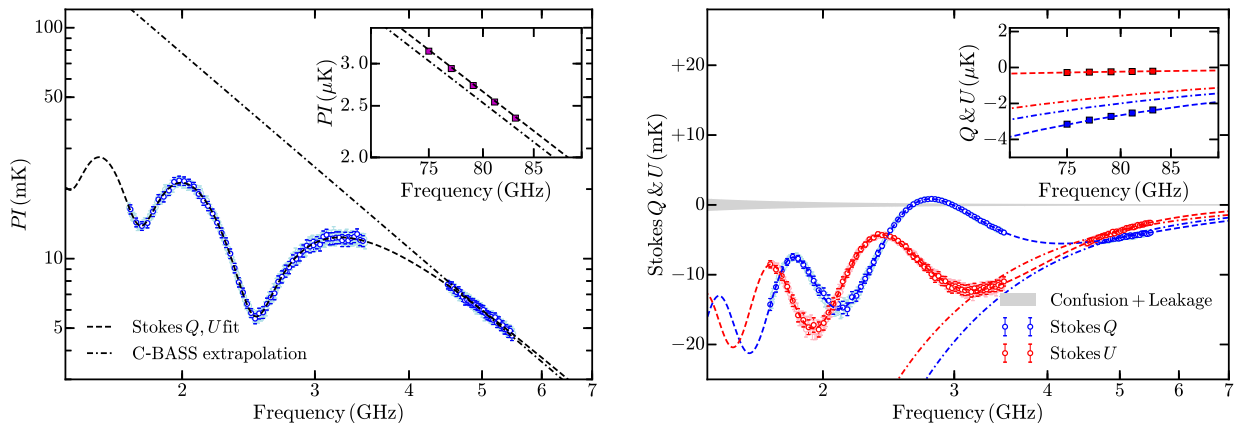


Figure 6. Left- and right-hand panels show the frequency spectrum of PI , and Stokes Q and U , respectively. The data points are generated from synthetic observations of a MHD simulation of isothermal compressible turbulence in the ISM. For clearer visual appearance, we have highlighted every fourth data point and the errorbars show 3σ . The dashed lines show the best fit model using Stokes Q, U fitting (listed in Table 2). The dot-dashed line show a simple power-law extrapolation of the polarized intensities measured with the C-Band data only. The shaded area represents confusion noise scaled to 1 degree angular resolution from polarized sources and an instrumental polarization leakage of 0.2%, added in quadrature. The insets show zoomed-in spectra around 80 GHz. These data were not used while performing the fit and should only serve as guides to evaluate the accuracy of the Stokes Q, U fitting technique.

Table 2. Best fit parameters for the three internal Faraday dispersion (IFD) components used as the model for Stokes Q, U fitting in Figs. 6 and 7.

Component Model	1 IFD	2 IFD	3 IFD
p_0	0.45 ± 0.01	0.11 ± 0.04	0.11 ± 0.04
FD_{em} (rad m $^{-2}$)	203.1 ± 0.7	71.7 ± 42.1	9.7 ± 14.9
σ_{FD} (rad m $^{-2}$)	14.2 ± 0.4	55.9 ± 18.2	21.5 ± 5.5
θ_0 (degree)	86.6 ± 1.0	-48.1 ± 14.3	88.6 ± 15.2

sky, a somewhat faint region to assess sensitivity to Faraday depolarization features in S-Band.

The data points in Fig. 6 shows the synthetic frequency spectrum of the linearly polarized intensity (PI) in the left-hand panel and, Stokes Q and U parameters in the right-hand panel. Note that large λ^2 coverage is essential for robust Stokes Q, U fitting, otherwise the fitted models and their parameters could be degenerate giving rise to systematic uncertainties. By combining S-Band data to C-Band data, the λ^2 coverage increases by a factor of about 20, i.e., from $\Delta\lambda^2 \approx 14.5 \text{ cm}^2$ in C-Band for the C-BASS to $\Delta\lambda^2 \approx 280 \text{ cm}^2$. We therefore combined S- and C-Band to perform Stokes Q, U fitting.

For this simulation, we are always looking at a Faraday rotating medium which is simultaneously synchrotron emitting. Also, there is no purely Faraday rotating medium in the foreground of the simulation volume. Therefore, in our case FD and FD_{em} are equivalent (see Section 4.2). For performing Stokes Q, U fitting, we have included various linear combinations of models of magneto-ionic media discussed in Section 4.2, including purely Faraday rotating media, and used the corrected Akaike information criteria (Hurvich & Tsai 1989; Cavanaugh 1997) to choose the preferred model.

For the example shown in Fig. 6, the best fit model was obtained for a linear combination of three internal Faraday dispersion components (Eq. 7) shown as the dashed lines

in Fig. 6. Best fit parameters are presented in Table 2. The dot-dashed line in the Fig. 6 shows a simple power-law extrapolation of the linearly polarized intensity measured at C-Band only. This is equivalent to assuming that the frequency-dependent Faraday depolarization at C-Band is negligible and the polarized intensity has the same spectral shape as that of the total synchrotron intensity (see e.g., Planck Collaboration X et al. 2016), in this example a power-law with $\beta_{nt} = -2.8$. A cursory look at the recovered Stokes Q and U parameters at C-Band using both the approaches appears to be in agreement within the errors. However, the technique of Stokes Q, U fitting captures the depolarization features imprinted on the polarized intensity spectrum at lower frequencies much better than the power-law approach. This information is crucial to estimate the contribution of the polarized synchrotron emission to the CMB foreground with cosmological precision.

The insets in Fig. 6 show the extrapolations around 80 GHz. The square data points show the expected polarized signal and were not included while fitting. The dashed and dot-dashed lines are the respective predictions of the linearly polarized synchrotron intensity around 80 GHz using Stokes Q, U fitting and assuming power-law spectrum from C-Band only measurements. Although the power-law extrapolation from the C-Band measurements well represents the polarized quantities around 80 GHz within sub- μK accuracy, the recovered Stokes Q and U parameters are significantly off. This is critical for measuring the polarization angle of the synchrotron emission. In order to accurately decompose the polarized CMB into E - and B -modes, errors in the polarization angle measurement of the foreground synchrotron emission could result in spurious mixing of the modes.

In Fig. 7, we show the polarization angle (θ) computed from the Stokes Q and U parameters in Fig. 6 (right-hand panel) as a function of frequency. The result of Stokes Q, U fitting is shown as the dashed line, simple extrapolation of

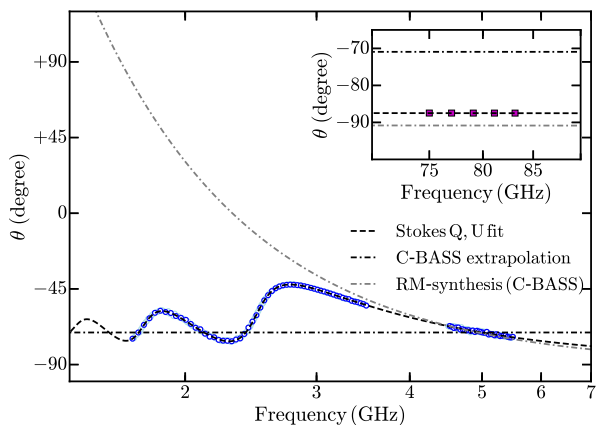


Figure 7. Variation of the polarization angle with frequency for the polarized emission shown in Fig. 6. Every fourth data point is highlighted for visual clarity. The dashed line shows the result of Stokes Q, U fitting, the black dot-dashed line shows the simple extrapolation of the polarization angle using the measurement at C-Band and the grey dot-dashed line shows the result of RM-synthesis applied to the C-Band only measurements.

the polarization angle measured by averaging over C-Band⁸ is shown as the black dot-dashed line and from RM-synthesis applied to the C-Band measurements is shown as the grey dot-dashed line. The inset shows the results of extrapolation in the vicinity of 80 GHz. It is obvious that a direct extrapolation from the C-Band averaged polarization angle does not recover the polarization angle around 80 GHz, and the estimated angles are off by more than 15° . Even by applying the technique of RM-synthesis to the C-Band only data, the recovered polarization angle is a couple of degrees off from the expected angle. This is mainly due to the fact that, low Faraday depth resolution of $\sim 2500 \text{ rad m}^{-2}$ at C-Band is insensitive to the complicated Faraday depth structures in the FD spectrum. In contrast, with the availability of S-Band data, Stokes Q, U fitting recovers the polarization angle at a fraction of degree accuracy. We however note that the accuracy of polarization angle measurement is limited by the accuracy to which the polarization angle of calibrators are typically measured and is about 1–2 degrees. Although Stokes Q, U fitting can recover the angle within fraction of a degree, systematic angle offsets due to uncertainty in the polarization angle of the calibrators cannot be excluded.

In Fig. 8 we show the extrapolated fractional polarization at 80 GHz using Stokes Q, U fitting to the combined S- and C-Band measurements as red points, and simple power-law extrapolation of the C-Band only measurements as the blue points, as a function of the expected fractional polarization at 80 GHz for a random set of sightlines. In this example, the C-Band only extrapolation suffers from systematic uncertainties up to $\sim -20\%$ with a mean of -10% , whereas the uncertainty using Stokes Q, U fitting is mostly statistical with up to $\sim \pm 10\%$ and has a dispersion of 5% around the expected fractional polarization at 80 GHz. In this exam-

⁸ To measure frequency averaged polarization angle, we first averaged the Stokes Q and U intensities over the C-Band and then computed the polarization angle.

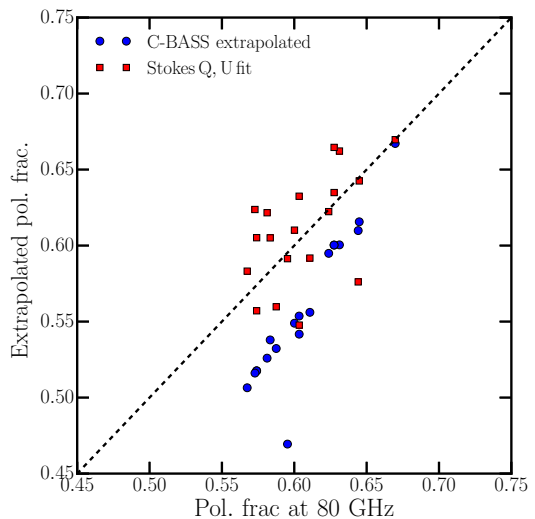


Figure 8. Extrapolated polarization fraction at 80 GHz as function of expected polarization fraction at 80 GHz determined from synthetic observations of MHD simulations. The red points are for the polarization fraction determined using the technique of Stokes Q, U fitting applied to combined S-Band and C-Band data. The blue points are for simple power-law extrapolation from observations at C-Band only. The errors on the data are smaller than the scatter.

ple, the intrinsic fractional polarization (p_0) and thereby the fractional polarization near 80 GHz are high (see Fig. 8) due to the relatively strong background magnetic field strength used in the MHD simulation. A lower ratio of the strengths of ordered to turbulent magnetic fields will lead to a lower p_0 for similar FD values used here. This will not change the overall results presented in this section.

We would like to point out that, the nature of systematic deviation of the C-Band extrapolated polarized emission discussed above might be a feature of the MHD simulation used by us as an example. A different set of simulation could lead to different systematics. This is being investigated with various type of MHD simulations of the turbulent ISM (A. Basu et al. in preparation). However, we do believe that using extrapolated C-Band only observations to model the foreground polarized synchrotron emission, can introduce undesirable systematics in the estimated polarized CMB map and therewith the polarized CMB angular power spectrum.

6.2.2 Regions of low Faraday depolarization

The example polarization spectra presented in the previous section show a region where frequency dependent Faraday depolarization is strong. In this section we discuss the properties of polarization spectra for a region where Faraday depolarization is less severe and representative of polarized emission from high Galactic latitudes. Unfortunately, we do not have access to MHD simulations for high galactic latitudes. Therefore, in order to mimic polarized emission from such regions, we simply scaled up the simulation volume used in the previous section. Magnetic field strengths were scaled using the assumption of magnetic flux freezing

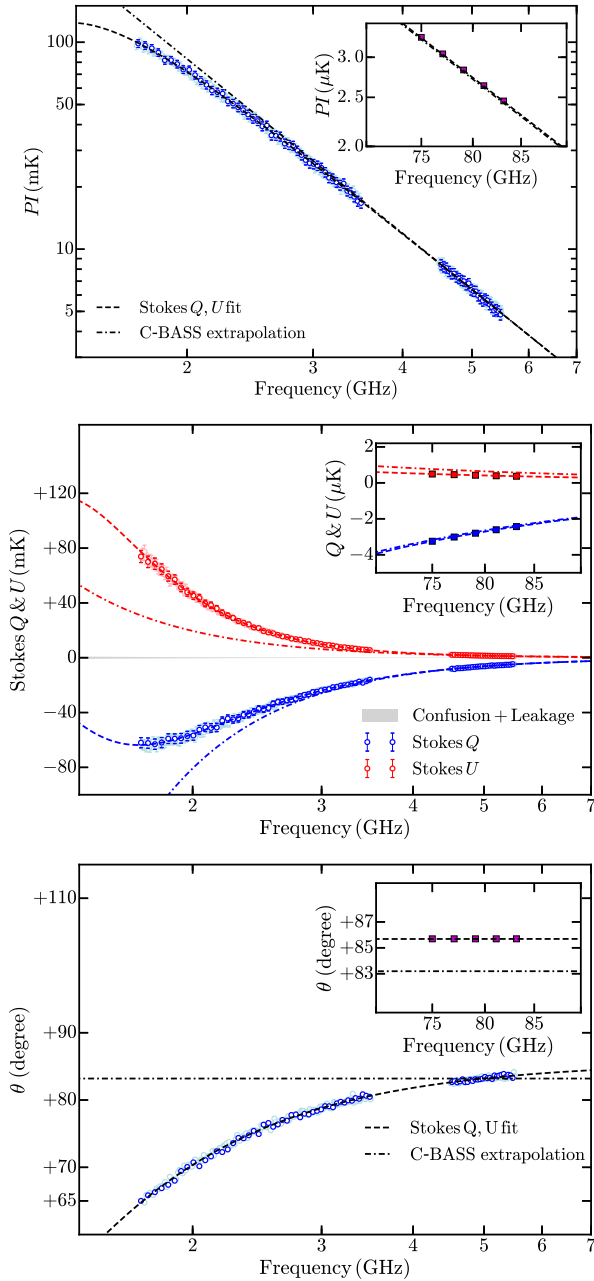


Figure 9. Example spectra of linear polarization parameters in a region where effects of Faraday depolarization is low. Top-, middle- and bottom-panels show the spectrum of PI , Stokes Q and U , and polarization angle, respectively. The points, lines and insets have the same meaning as the corresponding plots in Figs. 6 and 7.

and keeping the gas mass conserved. Thus, for our scaling, $B/\rho^{2/3}$ is conserved, where B is the magnetic field strength and ρ is the gas density.⁹ Here, we scaled the simulation volume to $1024 \times 1024 \times 1024 \text{ pc}^3$, i.e., a factor of 8 increase in

⁹ Strictly speaking, this approach does not represent the energetics and kinematics of actual physical conditions at high galactic latitudes, but is sufficient to extract synthetic polarization spectra with low Faraday depolarization.

Table 3. Best fit parameters for the two Burn slab components used as the model for Stokes Q, U fitting in Fig. 9

Component	1	2
Model	Burn	Burn
p_0	0.43 ± 0.02	0.16 ± 0.02
FD_{em} (rad m^{-2})	-32.3 ± 0.7	-2.2 ± 2.7
θ_0 (degree)	83.6 ± 0.8	-88.7 ± 1.8

volume of the original simulation. The median n_e in this case is 0.03 cm^{-3} and FD varies between -40 and $+40 \text{ rad m}^{-2}$ per $2 \times 2 \text{ pc}^2$ pixel. This represents the mid-Galactic latitude region, $30^\circ \lesssim |b| \lesssim 60^\circ$.

In Fig. 9 we show the frequency spectrum of quantities describing the linearly polarized emission averaged over a $30 \times 30 \text{ pc}^2$ region. The total synchrotron brightness is normalized to 1 K at 1 GHz. In this case, the best fit was obtained with a linear combination of two Burn slab components (Eq. 6) and the best fit parameters are listed in Table 3. From the top-panel of the figure, it is clear that both Stokes Q, U fitting and simple power-law extrapolation from C-Band measurements, recovers the polarized intensity near 80 GHz accurately. However, the approach of simple power-law extrapolation gives rise to slight systematic deviation in the extrapolated Stokes Q and U parameters as seen in the inset of the middle-panel in Fig. 9. This results in the polarization angle estimation near 80 GHz to be off by a few degrees (see inset in the bottom-panel of Fig. 9). In fact, in regions of low Faraday depolarization, performing Stokes Q, U fitting by combining C-BASS data with S-PASS will improve estimation of both polarized intensity and polarization angle with accuracy similar to what we find by combining broad-band S-Band data with C-BASS.

At high Galactic latitudes $|b| \gtrsim 60^\circ$, Faraday depolarization is expected to be even lower, and therefore extrapolation of polarization measurements in C-Band, e.g., from the C-BASS, by means of simple power-law, could recover the foreground polarized synchrotron emission at CMB frequencies quite well. Regions in the sky where such an extrapolation is applicable covers limited area. This thereby limits the measurement of angular power spectra of the polarized CMB at the largest angular scales. However, the method of Stokes Q, U fitting, by including S-Band measurements from the SKA-MPG telescope will give better accuracy, almost over the entire Southern sky.

7 POSSIBILITY OF QUIJOTE-LIKE COUNTERPART FOR THE SOUTHERN SKY

Currently the QUIJOTE experiment is being performed at the Teide observatory in Tenerife, Canary Islands to cover the Northern sky in the frequency range 11 to 40 GHz which aims to measure the Galactic AME and polarized dust emission (see Appendix A3). As mentioned in Jones et al. (2018), plans to extend QUIJOTE to the Southern hemisphere is not yet funded. The SKA-MPG telescope can also be equipped with Ku-band receivers operating in the frequency range 12 to 18 GHz equipped with a GPU based backend. This frequency coverage is similar to that of QUIJOTE's MFI and

would be ideal for conducting a QUIJOTE-like survey in the Southern hemisphere.

We however note that, since the SKA-MPG telescope was not originally designed for such an experiment, it has a small field of view (7 to 4.6 arcmin) because of a relatively large dish-size for a survey instrument at these frequencies (see Table 1). In order to achieve a sensitivity of $\sim 25 \mu\text{K}$, as targeted by the QUIJOTE experiment, ~ 10 min per resolution element will be required. This will lead to a total survey time of $\gtrsim 2 \times 60\,000$ hours to cover the Southern sky with the full 6 GHz (2×3 GHz) bandwidth of the SKA-MPG telescope in the Ku-Band. However, a smaller area on the sky, for example, the area of 2500 deg^2 covered by the South Pole Telescope (George et al. 2015) can be surveyed within a feasible time-scale of $\sim 10\,000$ hours using the SKA-MPG telescope. A study of the feasibility of such a survey by means of the SKA-MPG telescope is in progress and its results will be reported elsewhere.

8 DISCUSSION, OUTLOOK AND SUMMARY

The Galactic synchrotron and free-free emissions contribute significantly to the low-frequency CMB intensity foreground. Their separation is usually performed either via parametric foreground fits in each pixel (Planck Collaboration X et al. 2016), or via non-parametric template fits (Bennett et al. 2013). The success of the latter, among others, depends on the accuracy with which foreground templates can be obtained. For instance, $\text{H}\alpha$ maps, which serve as template for free-free emission, suffer from significant absorption by dust, especially around the Galactic plane up to $\pm 15^\circ$ in latitude, for which corrections have to be performed (see, e.g., Dickinson et al. 2003). The Haslam et al. (1982) all-sky survey at 408 MHz is considered as a template for the synchrotron emission (Planck Collaboration XXV et al. 2016). Alternatively, a combined parametric fit for all components is common practice (see, e.g., the Commander method in Planck Collaboration IV et al. 2018.). Here, however, degeneracies with other low-frequency foregrounds such as AME are inevitable, and due to their model uncertainties misidentification are likely.

Parametric pixel fits require assumptions on the spectral shape of the foregrounds considered, and possible degeneracies among different foregrounds, especially *above* ~ 10 GHz, must be controlled. Currently, due to the lack of suitable large sky-area surveys covering multiple frequencies below 10 GHz, modelling of the synchrotron spectrum is limited to minimal parametrization. For example, to estimate the contribution of the Galactic synchrotron emission at CMB frequencies, it is modeled as a perfect power-law with spectral index β_{nt} or with a constant spectral curvature over the entire sky by modifying β_{nt} as $\beta_{\text{nt}} + C \log(\nu/\nu_{\text{br}})$ (see e.g., Kogut 2012). Here, C is a curvature parameter. Such parametrizations do not adequately describe the physical nature of the synchrotron spectrum due to energy losses and propagation of the synchrotron emitting CREs discussed in Section 4.1.

Broad-bandwidth data at S-Band, along with other on-going surveys at slightly higher frequencies, like the C-BASS and QUIJOTE, provides the opportunity to describe the radio continuum spectrum with physically moti-

vated parametrization of the total synchrotron emission. We hereto suggest the parametrization presented in Section 4.1 and test its feasibility using simulated data in Section 6.1. More generally, we propose that large frequency coverage at frequencies *below* ~ 10 GHz has the advantage of constraining both synchrotron and free-free emission directly from the Galactic radio continuum spectrum alone. This thereby avoids degeneracies with the CMB itself, AME, CO emission and thermal dust, and circumvents uncertainties arising from templates.

In Section 6.1 we demonstrated the ability to constrain physical models of radio emission with the help of SKA-MPG telescope. We expect that a single, 300-hour S-Band survey of the Southern sky will provide a confusion limited intensity measurement resolved into 21 000 independent pixels with 200 frequency channels in each. Each single 300-hour survey when combined with surveys at higher frequencies will allow extrapolation of synchrotron and free-free emission to CMB frequencies with a rms brightness temperature uncertainty of less than $10 \mu\text{K}$ in most parts of the Galaxy. Survey at S-Band with the SKA-MPG telescope will be specially helpful to model curvature in synchrotron emission spectrum at high Galactic latitudes, $|b| \gtrsim 30^\circ$. For $|b| \lesssim 30^\circ$, our proposed method of simultaneous modeling of the synchrotron and free-free emissions will benefit from additional data in the frequency range 10 to 40 GHz. This in turn will lead to an increase of the fraction of sky that can be used for CMB analysis and thus help in reducing the limitations due to cosmic variance.

The full power of the planned S-Band survey however is revealed when we turn to the study of the polarized synchrotron emission with the SKA-MPG telescope, as discussed in detail in Section 6.2. Repeated 300 hours S-Band surveys are planned to eventually build up polarized maps with 0.3 mK sensitivity across 200 frequency channels spread over the S-Band.

From Figs. 6 and 7, it is clear that the technique of Stokes Q, U fitting is a powerful tool to estimate the linearly polarized emission, including the intrinsic polarization angle, of the foreground synchrotron emission which is often affected by Faraday depolarization. S-Band coverage using the SKA-MPG telescope is a valuable addition to applying this technique and does not suffer from model degeneracies as compared to higher frequency observations around C-Band. In fact, a deeper understanding of the foreground polarized emission through broad-band spectro-polarimetry is imperative to disentangle between local and cosmological structures. For example, residual signal of Galactic Loop I in the CMB's E -mode map has been hinted at in Liu (2018). The example MHD simulation we have used in Section 6.2.1 is representative of the ISM condition around the Galactic plane region extending to $\sim \pm 20^\circ$ in latitude and perhaps for the large-scale polarized loops and spurs extending to even higher/lower latitudes. As these regions are affected by severe Faraday depolarizations, they are usually masked from the polarized CMB angular power spectrum analysis. Stokes Q, U fitting is a powerful technique to model Faraday depolarization and thereby will increase the usable sky-area drastically.

Applying Stokes Q, U fitting to the combined S-Band data from the SKA-MPG telescope and C-Band data from the C-BASS, we expect to recover the polarization fraction

of the synchrotron emission near 80 GHz with a dispersion of 5% and achieve an accuracy better than a degree in estimating the angle of the linearly polarized synchrotron emission, even at $|b| \lesssim 30^\circ$. This is essential for reducing cosmic variance on the largest angular scales where the next-generation of CMB experiments are targeting to detect the imprints of primordial gravitational waves in the B -mode and effects of reionization history both in the E - and B -mode.

Future CMB space missions are aiming to constrain the B -mode peak for tensor-to-scalar perturbation power ratio r with sensitivity $\delta r < 0.001$ (Suzuki et al. 2018). This corresponds to rms of roughly 10 nK for the B -mode signal on 1 degree angular scales. In order to achieve these sensitivities, the polarized synchrotron emission in the foreground should be constrained with rms better than 5 nK at 100 GHz, i.e., better than ~ 10 nK at 80 GHz. Now, with 5% dispersion on polarization fraction estimation using Stokes Q, U fitting and $\lesssim 1$ μ K rms for the synchrotron emission estimation at 80 GHz,¹⁰ the rms of the polarized synchrotron emission is expected to be $\lesssim 10$ nK. This assumes a median intrinsic fractional polarization of 0.1 in regions of low Galactic latitudes $|b| < 30^\circ$. At higher $|b|$, the polarization fraction is expected to be higher, but synchrotron brightness and thereby the rms of its estimation is expected to be lower. We therefore expect that, applying Stokes Q, U fitting to data including the new broadband spectro-polarimetric measurements at S-Band would allow us to recover the polarized synchrotron foreground with rms better than 10 nK per 1 deg², over the entire Southern sky.

Further, the SKA-MPG telescope will be sensitive to point sources with flux densities $\gtrsim 300$ mJy beam⁻¹ at 2.5 GHz. As it will take about 20 survey cycles of about 300 hours each to reach the target sensitivity of ~ 0.3 mK in polarization, as a by-product SKA-MPG telescope will allow time-domain study of bright sources in all four Stokes parameters over 200 frequency channels in the S-Band.

Also, a Northern-sky counterpart of a similar S-Band survey is financially viable by procuring one of the SKA-MID dishes when they go into mass production and installing it in a RFI-quiet region in the Northern hemisphere. Availability of a Ku-band receiver covering the 12–18 GHz frequency range provides the possibility to extend QUIJOTE-like foreground studies to the Southern hemisphere. Thus, the SKA-MPG telescope will have strong impact on CMB foreground science addressing complimentary scientific aspects and help to expand existing dedicated surveys.

To summarize, a broad-band spectro-polarimetric survey in S-Band of the Southern sky with the SKA-MPG telescope will be crucial for estimating the synchrotron foreground, both total and polarized intensities, at frequencies where the CMB emission is expected to be relatively stronger. The survey with the SKA-MPG telescope will be sensitive to angular scales $> 1^\circ$ and will be complimentary to current on-going foreground measurement experiments. Broad-band spectro-polarimetry at S-Band will provide us the opportunity to apply, for the first time in studies of the Galactic foreground measurements, the powerful technique

of Stokes Q, U fitting, and constrain the synchrotron + free-free emission from the radio continuum observations alone. The technique of Stokes Q, U fitting is expected to play a crucial role in recovering the foreground polarized signal, both amplitude and polarization angle, at higher frequencies like 80–100 GHz, where next-generation, space-based CMB polarization anisotropy studies will be conducted, e.g., the *LiteBIRD* mission. These make the SKA-MPG telescope to have lasting and impactful scientific legacy.

ACKNOWLEDGEMENTS

We thank the anonymous referee for critical and constructive comments that have improved the content of the paper. We thank Eiichiro Komatsu and Olaf Wucknitz for valuable comments that have improved the presentation of this paper, and Pavel Naselsky and Carlo Baccigalupi for interesting discussions. We acknowledge financial support by the German Federal Ministry of Education and Research (BMBF) under grant 05A17PB1 (Verbundprojekt D-MeerKAT). BB acknowledges the generous support of the Simons Foundation. AB would like to thank Deutsche Bahn for its WIFIonICE and ICEportal services that enabled a significant portion of the text being written on-board than intended.

REFERENCES

- Abazajian K. N., et al., 2016, preprint, ([arXiv:1610.02743](https://arxiv.org/abs/1610.02743))
 Anderson C. S., Gaensler B. M., Feain I. J., 2016, *ApJ*, **825**, 59
 Armstrong J. W., Rickett B. J., Spangler S. R., 1995, *ApJ*, **443**, 209
 Basu A., Mitra D., Wadadekar Y., Ishwara-Chandra C. H., 2012, *MNRAS*, **419**, 1136
 Basu A., Beck R., Schmidt P., Roy S., 2015, *MNRAS*, **449**, 3879
 Bell A., 2004, *MNRAS*, **353**, 550
 Bennett C. L., et al., 1992, *ApJ*, **396**, L7
 Bennett C. L., et al., 2011, *ApJS*, **192**, 17
 Bennett C. L., et al., 2013, *ApJS*, **208**, 20
 Berkhuijsen E. M., 1972, *A&AS*, **5**, 263
 Bialy S., Burkhart B., Sternberg A., 2017, *ApJ*, **843**, 92
 Blandford R., Eichler D., 1987, *Phys. Rep.*, **154**, 1
 Brentjens M. A., de Bruyn A. G., 2005, *A&A*, **441**, 1217
 Burkhart B., Falceta-Gonçalves D., Kowal G., Lazarian A., 2009, *ApJ*, **693**, 250
 Burkhart B., Stanimirović S., Lazarian A., Kowal G., 2010, *ApJ*, **708**, 1204
 Burkhart B., Lazarian A., Gaensler B. M., 2012, *ApJ*, **749**, 145
 Burkhart B., Lazarian A., Ossenkopf V., Stutzki J., 2013, *ApJ*, **771**, 123
 Burn B. J., 1966, *MNRAS*, **133**, 67
 Caprioli D., Spitkovsky A., 2014, *ApJ*, **783**, 91
 Carretti E., et al., 2013, *Nature*, **493**, 66
 Carretti E., et al., 2019, preprint ([arXiv:1903.09420](https://arxiv.org/abs/1903.09420))
 Cavanaugh J. E., 1997, *Statistics & Probability Letters*, **33**, 201
 Cordes J. M., Lazio T. J. W., 2003, ArXiv Astrophysics e-prints
 Dickinson C., Davies R., Davis R., 2003, *MNRAS*, **341**, 369
 Edmon P., Kang H., Jones T., Ma R., 2011, *MNRAS*, **414**, 3521
 Elmegreen B. G., Scalo J., 2004, *ARA&A*, **42**, 211
 Frick P., Sokoloff D., Stepanov R., Beck R., 2011, *MNRAS*, **414**, 2540
 Gaensler B. M., et al., 2011, *Nature*, **478**, 214
 Génova-Santos R., et al., 2015a, in Cenarro A. J., Figueras F., Hernández-Monteagudo C., Trujillo Bueno J., Valdivielso L.,

¹⁰ Note that the rms on the total synchrotron emission estimated at 80 GHz is significantly lower than that of the synchrotron + free-free emission presented in Fig. 4.

- eds, Highlights of Spanish Astrophysics VIII. pp 207–212 ([arXiv:1504.03514](#))
- Génova-Santos R., et al., 2015b, *MNRAS*, **452**, 4169
- George E. M., et al., 2015, *ApJ*, **799**, 177
- Guo Z.-K., Schwarz D. J., Zhang Y.-Z., 2011, *Phys. Rev. D*, **83**, 083522
- Haslam C. G. T., Salter C. J., Stoffel H., Wilson W. E., 1982, *A&AS*, **47**, 1
- Haverkorn M., Brown J. C., Gaensler B. M., McClure-Griffiths N. M., 2008, *ApJ*, **680**, 362
- Heesen V., Dettmar R.-J., Krause M., Beck R., Stein Y., 2016, *MNRAS*, **458**, 332
- Heesen V., et al., 2018, *MNRAS*, **476**, 158
- Herron C. A., Burkhart B., Lazarian A., Gaensler B. M., McClure-Griffiths N. M., 2016, *ApJ*, **822**, 13
- Hinshaw G., et al., 2013, *ApJS*, **208**, 19
- Hurvich C. M., Tsai C.-L., 1989, *Biometrika*, **76**, 297
- Jaffe W., Perola G., 1973, *A&A*, **26**, 423
- Jelić V., et al., 2015, *A&A*, **583**, A137
- Jonas J. L., Baart E. E., Nicolson G. D., 1998, *MNRAS*, **297**, 977
- Jones T., 2011, *Journal of Astrophysics and Astronomy*, **32**, 427
- Jones M. E., et al., 2018, *MNRAS*, **480**, 3224
- Kang H., Edmon P., Jones T., 2012, *ApJ*, **745**, 146
- Kardashev N., 1962, *SvA*, **6**, 317
- Kim K. S., Lilly S. J., Miniati F., Bernet M. L., Beck R., O’Sullivan S. P., Gaensler B. M., 2016, *ApJ*, **829**, 133
- Klein U., Lisenfeld U., Verley S., 2018, *A&A*, **611**, A55
- Kogut A., 2012, *ApJ*, **753**, 110
- Kogut A., et al., 2003, *ApJS*, **148**, 161
- Koley A., Roy N., 2019, *MNRAS*, **483**, 593
- Kowal G., Lazarian A., Beresnyak A., 2007, *ApJ*, **658**, 423
- Krachmalnicoff N., et al., 2018, *A&A*, **618**, A166
- Krause M., et al., 2018, *A&A*, **611**, A72
- Krumholz M. R., Burkhart B., Forbes J. C., Crocker R. M., 2018, *MNRAS*, **477**, 2716
- Liddle A. R., 1994, *Phys. Rev. D*, **49**, 739
- Liu H., 2018, *A&A*, **617**, A90
- Loi F., Murgia M., Govoni F., Vacca V., Prandoni I., Bonafede A., Feretti L., 2019, *MNRAS*, **p. 395**
- Longair M., 2011, *High energy astrophysics*, 3rd ed. Cambridge: Cambridge University Press
- Lyth D. H., 1997, *Phys. Rev. Lett.*, **78**, 1861
- Mao S., Zweibel E., Fletcher A., Ott J., Tabatabaei F., 2015, *ApJ*, **800**, 92
- Mao S. A., et al., 2017, *Nature Astronomy*, **1**, 621
- O’Sullivan S., et al., 2012, *MNRAS*, **421**, 3300
- O’Sullivan S. P., Purcell C. R., Anderson C. S., Farnes J. S., Sun X. H., Gaensler B. M., 2017, *MNRAS*, **469**, 4034
- Oppermann N., et al., 2012, *A&A*, **542**, A93
- Oppermann N., et al., 2015, *A&A*, **575**, A118
- Pacholczyk A., 1970, *Radio astrophysics. Nonthermal processes in galactic and extragalactic sources*
- Paladino R., Murgia M., Orrú E., 2009, *A&A*, **503**, 747
- Park J., Caprioli D., Spitkovsky A., 2015, *Physical Review Letters*, **114**, 085003
- Pasetto A., Carrasco-González C., O’Sullivan S., Basu A., Bruni G., Kraus A., Curiel S., Mack K.-H., 2018, *A&A*, **613**, A74
- Penzias A. A., Wilson R. W., 1965, *ApJ*, **142**, 419
- Planck Collaboration I et al., 2018, preprint, ([arXiv:1807.06205](#))
- Planck Collaboration IV et al., 2018, preprint, ([arXiv:1807.06208](#))
- Planck Collaboration X et al., 2016, *A&A*, **594**, A10
- Planck Collaboration X et al., 2018, preprint, [p. arXiv:1807.06211](#) ([arXiv:1807.06211](#))
- Planck Collaboration XVI et al., 2016, *A&A*, **594**, A16
- Planck Collaboration XXV et al., 2016, *A&A*, **594**, A25
- Polnarev A. G., 1985, *Soviet Ast.*, **29**, 607
- Reich P., Reich W., 1986, *A&AS*, **63**, 205
- Schnitzeler D. H. F. M., 2018, *MNRAS*, **474**, 300
- Schwarz D. J., Copi C. J., Huterer D., Starkman G. D., 2016, *Classical and Quantum Gravity*, **33**, 184001
- Shneider C., Haverkorn M., Fletcher A., Shukurov A., 2014, *A&A*, **568**, A83
- Smoot G. F., et al., 1992, *ApJ*, **396**, L1
- Sokoloff D., Bykov A., Shukurov A., Berkhuijsen E., Beck R., Poezd A., 1998, *MNRAS*, **299**, 189
- Stil J. M., Keller B. W., George S. J., Taylor A. R., 2014, *ApJ*, **787**, 99
- Sun X. H., Han J. L., Reich W., Reich P., Shi W. B., Wielebinski R., Fürst E., 2007, *A&A*, **463**, 993
- Suzuki A., et al., 2018, *Journal of Low Temperature Physics*, **185**
- Tabatabaei F. S., et al., 2017, *ApJ*, **836**, 185
- Testori J. C., Reich P., Reich W., 2008, *A&A*, **484**, 733
- Thorne B., Dunkley J., Alonso D., Naess S., 2017, *MNRAS*, **469**, 2821
- Uyaniker B., Fuerst E., Reich W., Reich P., Wielebinski R., 1998, *A&AS*, **132**, 401
- Wolleben M., Landecker T. L., Reich W., Wielebinski R., 2006, *A&A*, **448**, 411
- Wolleben M., et al., 2009, in Strassmeier K. G., Kosovichev A. G., Beckman J. E., eds, *IAU Symposium Vol. 259, Cosmic Magnetic Fields: From Planets, to Stars and Galaxies*. pp 89–90 ([arXiv:0812.2450](#)), [doi:10.1017/S1743921309030117](#)
- Zaldarriaga M., Seljak U., 1997, *Phys. Rev. D*, **55**, 1830

APPENDIX A: LARGE SKY-AREA BROAD-BANDWIDTH SURVEYS

Several radio frequency surveys covering large sky areas have been performed in the past using narrow frequency bands, mainly to study the Galactic radio continuum and polarized emission, and hence are not optimum to achieve required sensitivities for CMB foreground separation (see Section 3). Further, following the results of previous dedicated CMB foreground measurement surveys by the *WMAP* satellite at frequencies above 22.8 GHz and by the *Planck* satellite at frequencies above 28.4 GHz, it has become abundantly clear that reliable measurements of the Galactic synchrotron emission are best performed at frequencies between 2 and 20 GHz (Planck Collaboration X et al. 2016).

In this section we discuss in brief the salient features of recent and on-going efforts to measure the polarized Galactic foreground emissions.

A1 C-BASS

The C-Band All Sky Survey (C-BASS) is a survey aimed at mapping the entire sky, both in total and polarized intensities, at 5 GHz (C-Band) with 45 arcmin angular resolution (Jones et al. 2018). To cover the entire sky, C-BASS is being performed with two telescopes located in North and South hemispheres. In the North, a 6.1-m Gregorian telescope will map the sky for declinations $> -15^\circ.6$. This telescope uses a receiver at a frequency centred at 4.783 GHz averaging signal over a bandwidth of 0.499 GHz. In the South, a 7.6-m Cassegrain telescope will survey the sky for declination $< 28^\circ.6$ and is equipped with a receiver capable of recording 1 GHz bandwidth split over 128 frequency channels centred at 5 GHz. To our knowledge, the C-BASS Southern survey is the first dedicated survey for measuring

the foreground polarized emission contaminating the CMB through broad-bandwidth radio spectro-polarimetry.

A2 S-PASS

The S-Band Polarization All Sky Survey (S-PASS) is the only other spectro-polarimetric survey at S-Band. It was performed using the Parkes 64-m telescope at 9 arcmin angular resolution (Carretti et al. 2019). The survey was performed using a relatively narrow bandwidth of 256 MHz centred at 2.3 GHz with 512 frequency channels binned into 8-MHz wide channels. Due to radio frequency interference, effectively 184 MHz of the band was usable in the frequency ranges 2.176 to 2.216 GHz and 2.256 to 2.4 GHz. This makes direct fitting of the Stokes Q , U data difficult due to degeneracy between fitting models and their parameters, especially in regions of strong Faraday depolarization. Also, application of RM-synthesis, even when combined with the C-BASS Southern sky data, will give rise to strong sidelobes in the Faraday depth spectrum due to a large gap in λ^2 -space (see Fig. 5). This will make it difficult to discern complicated Faraday depth features and/or multiple Faraday depth components.

A3 QUIJOTE

The Q-U-I-Joint TENERIFE (QUIJOTE) is an experiment designed to measure polarized foregrounds to constrain the B -mode polarization of CMB in the Northern sky (Génova-Santos et al. 2015a,b). A multi-frequency instrument (MFI) covers the frequency range 10–20 GHz centred at 11.2, 12.9, 16.7 and 18.7 GHz with 4 horns. The angular resolution at the two lower frequencies is 0.92° and at the two higher frequencies is 0.60° . At these frequencies the foreground continuum emission is expected to be dominated by the anomalous microwave emission (AME) making QUIJOTE less suitable for constraining the Galactic synchrotron emission. Moreover, the deep survey of QUIJOTE for cosmological studies is designed to target smaller sky area covering around 3000 deg^2 . Thus, QUIJOTE will be important to glean complimentary information on foreground AME emission in contrast to C-BASS and our planned survey at S-Band.

A4 GreenPol

The GreenPol experiment is another effort for measuring the Galactic polarized emission at frequencies 10, 15, 20, 30 and 44 GHz (Fuskeland et al., in preparation).¹¹ Located at the Summit Station in Greenland, the GreenPol can survey upto $\sim 50\%$ of the sky with angular resolutions ranging from 80 arcmin at the lowest frequency to ≈ 18 arcmin at the highest frequency. Similar to QUIJOTE, GreenPol experiment will be sensitive for studying AME.

¹¹ <https://www.deepspace.ucsb.edu/projects/greenpol>

A5 Surveys below 2 GHz

The GALFA Continuum Transit Survey¹² (GALFACTS) and the Global Magneto-Ionic Medium Survey (GMIMS; Wolleben et al. 2009) are two large sky-area, spectro-polarimetric surveys conducted at frequencies below 2 GHz. GALFACTS is performed with the 300-m Arecibo telescope covering the frequency range 1.225 to 1.525 GHz. The 300 MHz wide bandwidth is split into 1024 channels. Since, GALFACTS is a transit survey, it covers limited sky area which is not conducive for CMB foreground studies. GMIMS, however, will cover the entire sky in the frequency range 0.3 to 1.8 GHz subdivided into low-band, covering 0.3 to 0.9 GHz, mid-band, covering 0.9 to 1.3 GHz, and high-band, covering 1.3 to 1.8 GHz. In the high-band, observations are performed with the DRAO 26-m telescope in the north and Parkes 64-m telescope in the South.¹³ The low-band survey for the Southern sky was performed using the Parkes 64-m telescope. The mid-band, 0.9 to 1.3 GHz, is not yet covered.

Although, at these frequencies the Faraday depths can be estimated with better accuracy as compared to higher frequency measurements, Faraday depolarization effects are severe. Typically, depolarization increases as λ^4 making the polarized signals at $\sim 1.5 \text{ GHz} \gtrsim 16$ times more depolarized than at $\sim 3 \text{ GHz}$ which results in lower frequency observations being sensitive to local polarized structures (Jelić et al. 2015). This is a major concern when combining the polarization data from frequencies $\lesssim 1 \text{ GHz}$ with that from higher frequencies ($\gtrsim 5 \text{ GHz}$, e.g. the C-BASS data), because the emitting volume probed at the two frequency regimes could be significantly different.

This paper has been typeset from a $\text{\TeX}/\text{\LaTeX}$ file prepared by the author.

¹² <https://www.ucalgary.ca/ras/GALFACTS>

¹³ The Southern-sky component of GMIMS is known as the Southern Twenty-cm All-sky Polarization Survey (STAPS).

